Annual Report, NASA Contract NASW-96030

Biospheric Effects of the Chicxulub Impact and Their Role in the Cretaceous/Tertiary Mass Extinction

Kevin O. Pope
Geo Eco Arc Research
2222 Foothill Blvd., Suite E-272, La Canada, CA 91011

August 14, 1997

SUMMARY

A comprehensive analysis of volatiles in the Chicxulub impact strongly supports the hypothesis that impact-generated sulfate aerosols caused over a decade of global cooling, acid rain, and disruption of ocean circulation, which contributed to the mass extinction at the Cretaceous/Tertiary (K/T) boundary. The crater size, meteoritic content of the K/T boundary clay, and impact models indicate that the Chicxulub crater was formed by a short period comet or an asteroid impact that released 0.7-3.4 x 10^{31} ergs of energy. Impact models and experiments combined with estimates of volatiles in the projectile and target rocks predict that over 200 gigatons (Gt) each of SO_2 and water vapor, and over 500 Gt of CO_2, were globally distributed in the stratosphere by the impact.

Additional volatiles may have been produced on a global or regional scale that formed sulfate aerosols rapidly in cooler parts of the vapor plume, causing an early, intense pulse of sulfuric acid rain. Estimates of the conversion rate of stratospheric SO_2 and water vapor to sulfate aerosol, based on volcanic production of sulfate aerosols, coupled with calculations of diffusion, coagulation, and sedimentation, demonstrate that the 200 Gt stratospheric SO_2 and water vapor reservoir would produce sulfate aerosols for 12 years. These sulfate aerosols caused a second pulse of acid rain that was global.

Radiative transfer modeling of the aerosol clouds demonstrates (1) that if the initial rapid pulse of sulfate aerosols was global, photosynthesis may have been shut down for 6 months and (2) that for the second prolonged aerosol cloud, solar transmission dropped 80% by the end of first year and remained 50% below normal for 9 years. As a result, global average surface temperatures probably dropped between 5° and 31°K, suggesting that global near-freezing conditions may have been reached. Impact-generated CO_2 caused less than 1°K greenhouse warming and therefore was insignificant compared to the sulfate cooling. The magnitude of sulfate cooling depends largely upon the rate of ocean mixing as surface waters cool, sink, and are replaced by upwelling of deep ocean water. This upwelling apparently drastically altered ocean stratification and circulation, which may explain the global collapse of the delta ^{13}C gradient between surface and deep ocean waters at the K/T boundary.

A review of geological studies of the Cretaceous/Tertiary boundary provides ample evidence for sulfur degassing and acid rain immediately following the impact. The few quantitative measurements of this degassing and acid rain match well with the impact model predictions. Geological evidence for global cooling and changes in ocean circulation also match impact predictions, however they lack the temporal resolution needed to test the duration of the sulfate loading. Prolonged global changes caused by the impact may be linked to the effects of sulfate cooling on ocean circulation, which once perturbed, may have required nearly 1 million years to recover.

The most proximal exposures of ejecta from the Chicxulub impact crater are found on Albion Island and in the Cayo District of Belize. On Albion Island, these ejecta deposits are composed of two units: 1) a basal, ~1-m-thick clay and dolomite Albion Spheroid Bed overlying Late Cretaceous carbonate platform sediments; and 2) an upper ~15-m-thick coarse Albion Diamictite Bed with allochthonous boulders up to 7.5 m in diameter. Analysis of the clay spheroids indicates that they are altered glass. The dolomite spheroids commonly have concentric layers and angular cores consistent with an accretionary lapilli origin. An iridium concentration (111-152 parts/trillion), five times above background, was detected in the base of the Spheroid Bed associated with abundant altered glass

spheroids. The Diamictite Bed contains ~10% clay that we interpret as mostly altered glass, rare shocked quartz, and striated and polished dolomite cobbles, one with a penetrating rock chip that impacted under pressures sufficient to have plastically deformed the cobble. In central Belize, ejecta deposits contain abundant limestone pebbles and cobbles (Pook's Pebbles) with polish, striations, and penetrating rock chips similar to the dolomite ones noted above. SEM images of the striated and polished surfaces indicate particle interactions under high temperature and partial melting of the surface.

The Albion Spheroid Bed is interpreted as deposited from the lateral blast of the vapor plume. This plume entrained small particles as it passed through the ejecta curtain, many of which grew by accretion before deposition. The Albion Diamictite Bed is interpreted as the result of a turbulent flow that contained debris derived from the ejecta curtain, analogous to the fluidized ejecta blankets on Mars. The Pook's Pebbles from Cayo are interpreted as high-altitude ballistic ejecta that have undergone ablation during atmospheric reentry.

IMPACT MODELING

Target Properties

Recent studies of drill cores from the rim of the Chicxulub crater indicate that the approximately 3 km thick sequence of sediments present at the time of impact (Figure 1) was composed of 35-40% dolomite, 25-30% limestone, 25-30% anhydrite, and 3-4% sandstone and shale (Ward et al., 1995). For our study we assume 70% carbonate (limestone and dolomite) and 30% anhydrite, other lithologies being negligible. Exact water depths at the time of impact remain uncertain, but the limited core data combined with sea level trends within the Gulf of Mexico suggest that water depths were minimal. We assume no appreciable open water existed at the time of impact. Since a large amount of water was present as pore water in the carbonates (average 20% porosity, equivalent to ~420 m water depth), a few tens of meters of surface water, if present, would be negligible in our impact calculations.

Impact Vaporization of Sediments

In this study, we adopt values of 70 GPa for the complete vaporization of carbonate and 100 GPa for the complete vaporization of anhydrite (Badjukov et al., 1995; Yang et al., 1996). For water, we adopt a vaporization pressure of 10 GPa, based on the calculations of Kieffer for the impact vaporization of water contained within rock pore space (Kieffer and Simonds, 1980; Alvarez et al., 1995).

Crater Size

The final crater diameter (D_f) is not related to impact energy in a straightforward way, and most researchers scale impact energy with the transient crater diameter (D_{tc}, the diameter of the bowl-shaped cavity that forms immediately after impact prior to collapse of the rim and rebound of the crater floor).

The recent analysis of the surface expression of Chicxulub by Pope et al. (1996) suggests that much of the buried crater morphology is reflected in subtle topographic features (Figure 1). We interpret Chicxulub as a peak ring structure, where a concentric topographic ridge with a radius of

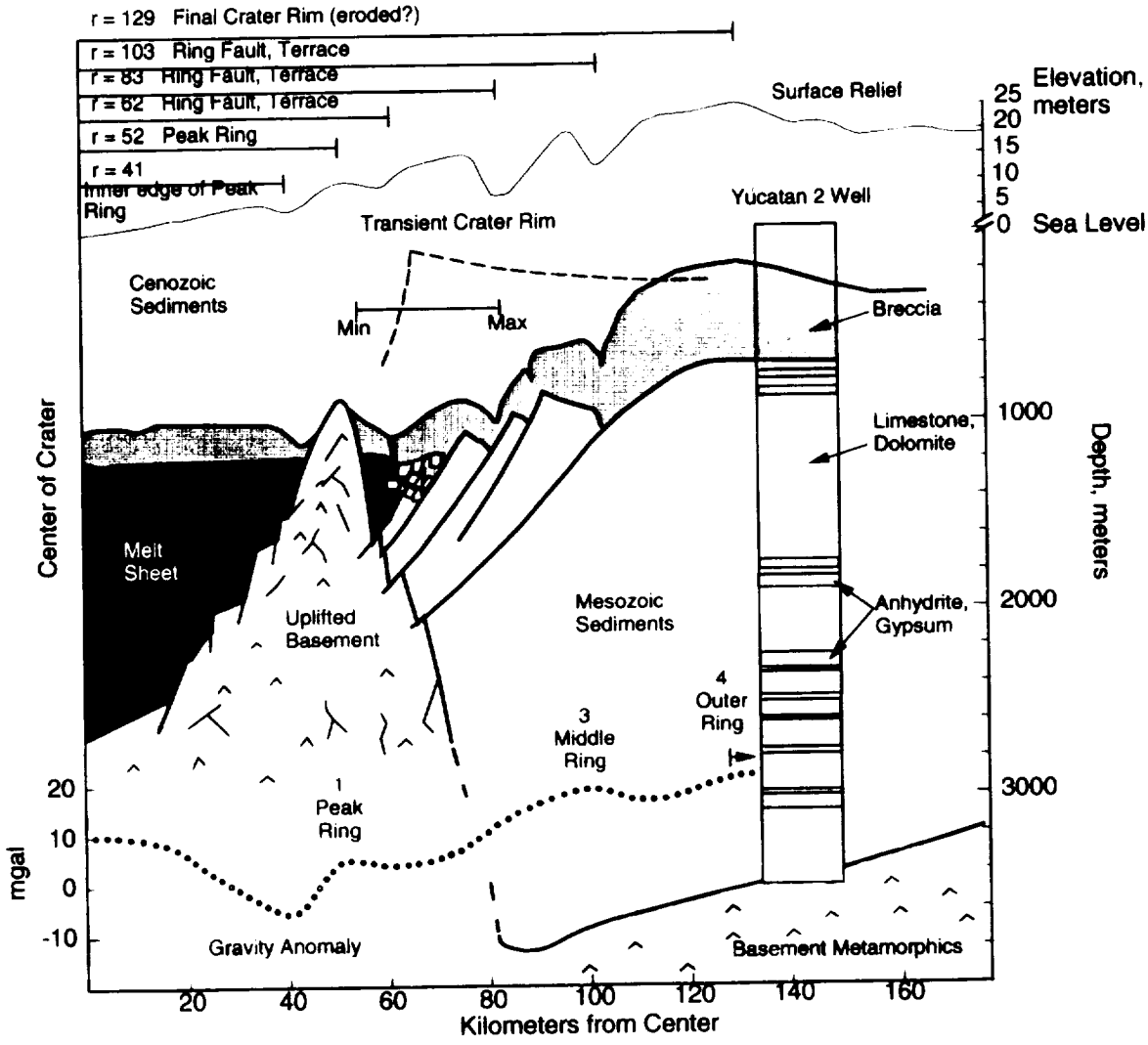

Figure 1. Structure, target lithology, and surface expression of the Chicxulub crater (southeastern half) based on (1) interpretations of topographic features from Pope et al. (1996), (2) well data from Ward et al. (1995) and Marin and Sharpton (1996), and (3) interpretations of gravity data from Sharpton et al. (1993, 1996). This reconstruction is similar to that of Sharpton et al. (1996). Note large vertical exaggeration and change in scale above and below sea level. Gravity anomaly data are average values from Sharpton et al. (1993). Position of transient crater rim (dashed line) is based on discussion by Croft (1985), where the minimum (min) and maximum (max) rim radii are shown, constrained by the peak ring and the prominent terrace scarp at a radius ~83 km indicated by the topography and location of the cenote ring.

129±5 km corresponds with the buried crater rim, indicating a D_f of ~260 km. This diameter is slightly larger than the D_f of 240 km we proposed earlier based on scaling from the inferred crater floor and limited coring (Pope et al., 1993), although the 260 km topographic rim may be eroded back from its original position. We identified a surface trough feature at a radius of 62±5 km, which we interpret as the surface expression of a ring fault marking the innermost terrace. A roughly concentric topographic ridge, which we interpret as the surface expression of the buried peak ring (radius ~52 km), lies between the previously mentioned 62 km radius trough and another inner trough at 41±2 km. We infer additional ring faults at radii of 83±3 km and 103±6 km, based on the presence of other concentric troughs. The 83 km radius trough is the most pronounced topographic feature and contains a semicircular chain of sink holes (Cenote Ring). The terrain rises abruptly from this trough to the ridge crest at a ~129 km radius.

Croft's (1985) analysis of large complex craters places the transient crater rim just within the inner-most terrace and outside of the peak ring. Using our topographic analysis and Croft's criteria we infer a D_{tc} for Chicxulub of ~130 km (Figure 1), which agrees well with a D_{tc} of 125 km predicted by Croft's power function scaling of a 260 km diameter terrestrial crater formed in sedimentary rocks. Given the location of a major buried structural feature indicated by the concentric ~83 km trough, and Croft's (1985) placement of the transient crater rim near the innermost terrace, we find it unlikely that D_{tc} exceeds ~165 km.

In overview, we find that the best estimates for the D_f and D_{tc} of Chicxulub are 260 km and 130 km, respectively. These findings are not definitive, however, and until more data are acquired, we suggest that for scaling purposes a range of values, $110 \leq D_{tc} \leq 165$ km, be considered (Figure 1). D_{tc} values outside of this range are inconsistent with the topographic and geophysical data.

Energy of the Chicxulub Impact

Measurements of the amount of meteoritic material contained in the K/T boundary indicate a projectile mass of 450-980 Gt (Kyte et al., 1985), which corresponds to a chondritic asteroid diameter of ~7-10 km, if the entire projectile was deposited in the K/T boundary clay. Calculations presented by Vickery and Melosh (1990) suggest that for a 14 km diameter asteroid impacting at 20 km/s little of the asteroid mass may be lost to space, but for the same projectile impacting at 35 km/s, 80% may be lost. Hence, if Chicxulub were formed by a ~35 km/s impact, the conservative estimates of meteoritic material by Kyte et al. (1985) are most consistent with an asteroid 14-20 km in diameter.

Our analysis of the size of the transient crater, coupled with the amount of meteoritic material in the K/T boundary layer, indicate that the projectile diameter was in the range of 9.4 km (32 km/s asteroid) to 24 km (25 km/s comet) (Figure 2). These parameters corresponds to an impact energy range of about 6.7×10^{30} to 3.4×10^{31} ergs. No typical asteroid (20 km/sec, density 2-3 g/cm^3) could have formed the Chicxulub crater, as only asteroids with velocities ≥25 km/sec fit the coupled constraints shown in Figure 2. No long-period comet (velocity >45 km/s) can be accommodated either, a result also found by Vickery and Melosh (1990) based an analysis similar to ours. It is also important to note that our analysis shown in Figure 2 is based upon scaling for a vertical impact. Oblique impacts create slightly smaller craters (Melosh, 1989, p. 121), but the diameter and depth dependence on impact angle is not well constrained. If Chicxulub were a highly oblique impact, then the projectile diameter, velocity, and energy may have been slightly larger than we propose.

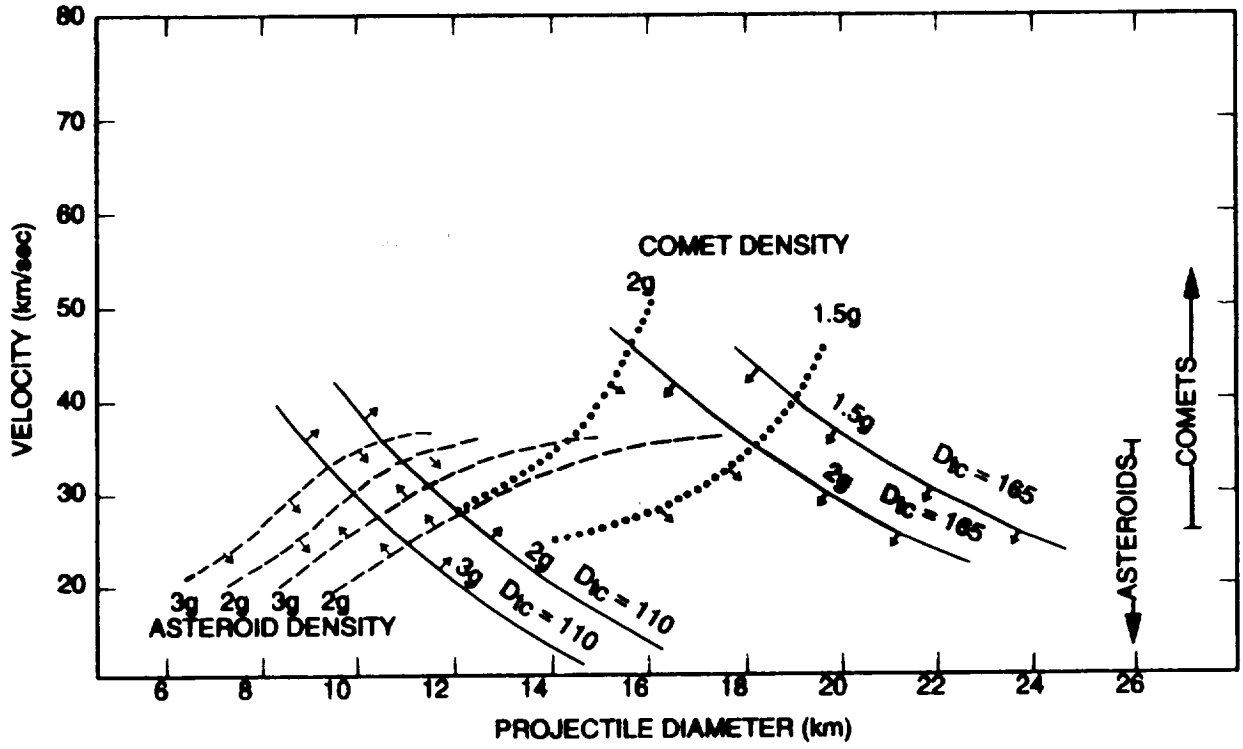

Figure 2. Constraints on the size and velocity of the comet or asteroid that formed the Chicxulub crater. Asteroids are assumed to have impact velocities <35 km/s, and comets >25 km/s. Solid lines present diameter-velocity minima (arrows pointing to the upper right) and maxima (arrows pointing to the lower left) constrained by the range of possible transient crater diameters ($110 \leq D_{tc} \leq 165$ km). Calculations are based on projectile densities of 1.5-3.0 g/cm^3 (1.5g-3g), assume a vertical impact, and use the Schmidt-Holsapple scaling relation presented by Melosh (1989, p. 121). Dashed lines present diameter-velocity minima (arrows pointing to the lower right) and maxima (arrows pointing to the upper left) constrained by the minimum (450 Gt) and maximum (980 Gt) mass estimates of the meteoritic material retained by Earth. Maxima and minima are given for asteroid densities of 2 and 3 g/cm^3 (2g, 3g) and calculations are based on the K/T boundary meteoritic mass estimates of Kyte et al. (1985) combined with the estimates of Vickery and Melosh (1990) for the amount of meteoritic material retained for an impact with a given projectile mass and velocity. Calculations assume all the retained projectile mass is globally distributed. Dotted lines present comet diameter-velocity minima imposed by the K/T boundary meteoritic mass for comets composed of 50% ice, density 1.5 g/cm^3 (1.5g) and 25% ice, density 2.0 g/cm^3 (2g). The same criteria used for asteroids were used for comets, although the maximum comet size is constrained by the crater size. Dark (asteroid) and light (comet) stippled areas correspond to the range of possible projectile parameters. At the top of the figure is a summary of the range of possible asteroid and comet diameters based on the constraints depicted (slightly larger diameters or velocities may be possible if the impact was highly oblique; see text).

Evolution of the Chicxulub Vapor Plume

Our estimates of the mass of volatiles injected into the atmosphere by the Chicxulub impact are based on Ivanov's earlier two-dimensional hydrocode model of the Chicxulub impact (Pope et al., 1994; Ivanov et al., 1996). This model provides estimates of the volumes of Mesozoic sediment shocked to within specific pressure ranges, which when coupled with our estimates of target composition and vaporization thresholds presented above, allow us to calculate volatile masses (Table 1). These masses are calculated for two domains: the footprint, corresponding to the region immediately beneath the projectile, and the out-of-footprint, corresponding to the region of shocked sediments outside the direct path of the projectile (Figure 3).

The importance of the distinction between these two domains lies in the evolution of the vapors. The footprint material first travels down into the transient crater, where it is mixed with highly shocked silica-rich basement rocks, and is ejected with the hottest vapors many seconds after initial impact (Ivanov et al., 1996). The out-of-footprint material begins to degas within 1-2 s after impact and is ejected in a less hot part of the vapor plume. Alvarez et al. (1995) refer to these two portions of the plume as the "hot fireball" (footprint) and "warm fireball" (out-of-footprint).

The vapors in the warm fireball are dominated by H_2O, with small amounts of CO_2 and SO_2 (Table 1) and do not contain much silicate vapor. The temperature of the warm fireball may not exceed 2000°K, and with rapid expansion of the vapors, much of the gas may not reach thermodynamic equilibrium. Under these conditions of moderate temperatures and rapid expansion, some of the vaporized sulfates may evolve as SO_3, not SO_2, as indicated by thermodynamic models (Lyons and Ahrens, 1996) and by laser vaporization experiments (Gerasimov et al., 1994, 1995; Ivanov et al., 1996). The initial expansion of the warm fireball would occur in direct contact with rock fragments of the ejecta curtain (e.g., Alvarez et al., 1995). The warm fireball would be highly turbulent where it interacted with the ejecta and atmosphere. Presumably, some mixing with the hot fireball would occur, but since the hot fireball develops many seconds later, the warm fireball could expand 100 km prior to the initial expansion of the hot fireball. The warm fireball probably condenses much more rapidly than the hot fireball, given its lower initial temperature. Condensation may lead to the precipitation of carbonate, as has been suggested for the origin of carbonate spherules found in Belize (Figure 3) (Ocampo et al., 1996a, see also ejecta section below), or of sulfates (including sulfuric acid), as has been demonstrated with laser vaporization experiments (Gerasimov et al., 1994, 1995; Ivanov et al., 1996). Water condensation would not occur as rapidly given its low vaporization temperature and the residual heat of the warm fireball combined with the heating of the stratosphere by the reentry of ejecta (see discussion in next section). Thus water vapors would be widely dispersed, perhaps globally.

The hot fireball is comparable to the K/T vapor plume modeled by several investigators (e.g., Vickery and Melosh, 1990; Zahnle, 1990) and is somewhat similar to the fireball modeled for the Shoemaker-Levy 9 comet impact with Jupiter (e.g., Takata et al., 1994; Zahnle and Mac Low, 1994; Zahnle et al., 1995). These impact plume studies demonstrate that the vapors in the hot fireball rapidly blow out of the top of the atmosphere and spread, in the K/T case, around Earth.

Baseline Volatile Masses

Estimates of the CO_2, SO_2, and H_2O masses from within the projectile are not included in Table 1. Recent impact models suggest that as little as 20% of a 10 km diameter asteroid is vaporized in a 20 km/s impact (Pierazzo et al., 1996). Most of the projectile may be vaporized in high-velocity

Table 1. Target Volatile Mass Injected Into Atmosphere

Crater Diameter D_A	Projectile		SO_2*			CO_2†			H_2O‡		
	Diameter,	Velocity,	Gt (10^{15} g)			Gt (10^{15} g)			Gt (10^{15} g)		
km	km	km/s	F	OF	Total	F	OF	Total	F	OF	Total
180	10	20	98	16	114	159	48	207	32	280	312
220	12	25	140			234			48		
300	14	38	192	65	257	317	207	524	70	400	470
300	16	30	247			416			84		
300	18	25	313			527			107		
300	20	20	384	33	417	648	97	745	133	400	533
300	22	25	467			787			160		
300	24	25	556			936			190		

F, vapors from footprint; OF, vapors from out-of-footprint, based on shocked volumes from Ivanov et al. [1996]. Hydrocode model grid size prevented accurate calculations of OF water vapor mass for craters >180 km. The 400 Gt estimates are extrapolations of the calculations provided by Ivanov et al. [1996] and are considered minimum values. Crater diameters are approximate.

*Based on 3 km thick section with 30% anhydrite at 2.9 g/cm3 (41% SO_2 by volume) shocked 100 GPa.

†Based on 3 km thick section with 70% carbonate with 20% porosity at 2.8 g/cm3 (69% CO_2 by volume) shocked 70 GPa.

‡Based on water in 20% porosity in 2.1 km thick carbonate section at 1.0 g/cm3 (14% H_2O by volume) shocked 10 GPa.

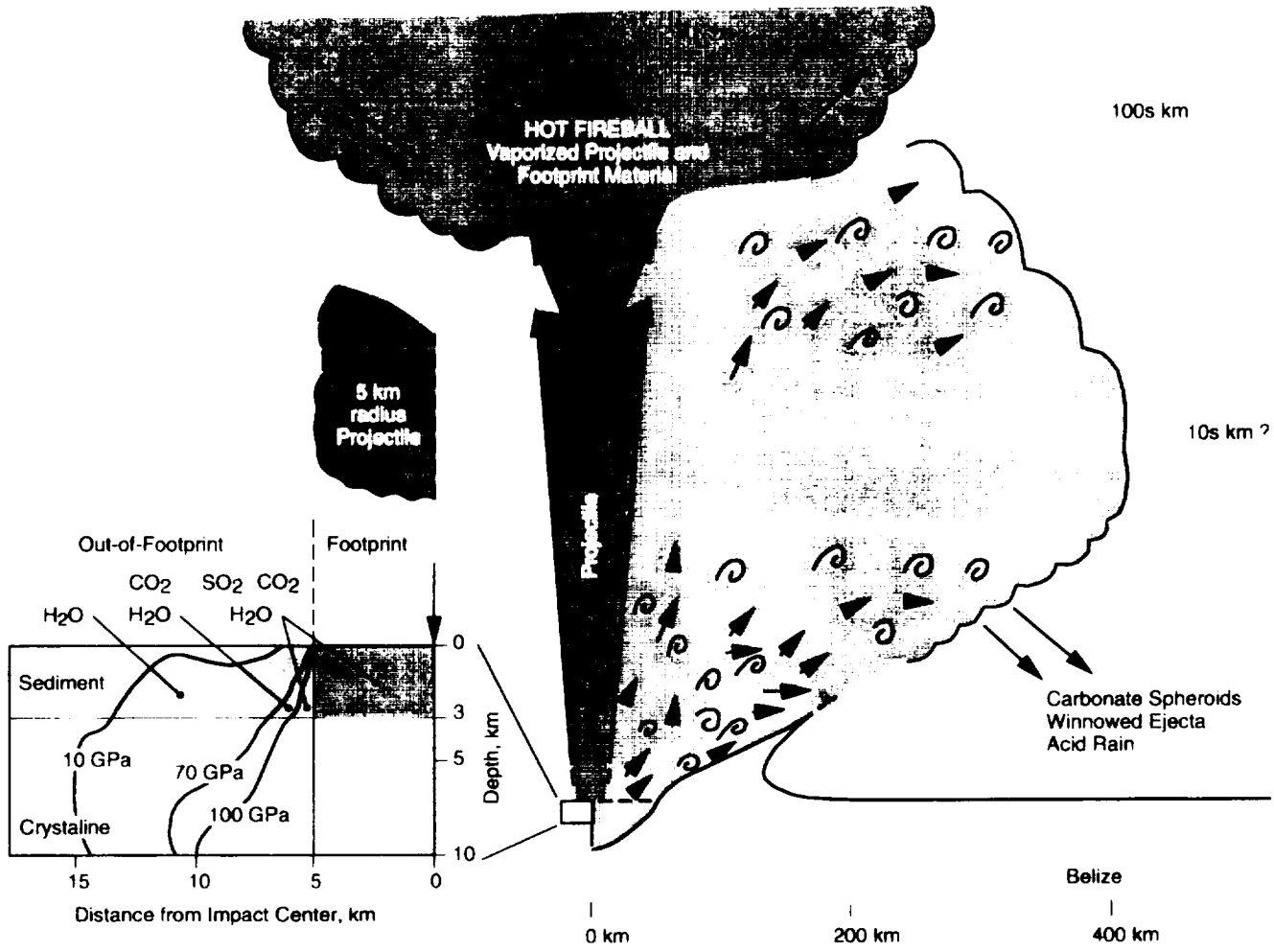

Figure 3. Model of vapor plume formation. Left side of diagram shows results of 2-D hydrocode model (left half only of symmetrical model) of a vertical impact of a 10 km diameter, 20 km/s, asteroid into a wet sedimentary layered target (adapted from Pope et al. (1994) and Ivanov et al. (1996)). Shown are the footprint and out-of-footprint regions with shock pressures (in GPa) and respective volatile species that are released. The right side of the diagram presents a schematic view of the origin and trajectories of the hot and warm fireballs that evolve from the footprint and out-of-footprint regions, respectively. The hot fireball blows out of the upper atmosphere and is distributed globally (in high-velocity impacts some material is ejected out of Earth orbit). Part of the warm fireball may also blow out of the upper atmosphere and spread globally, but a portion expands laterally, passing through the ejecta curtain, altering the trajectories of the finer ejecta. This lateral blast slows and cools rapidly, depositing particles that condense and coagulate in the plume: a possible origin of the carbonate spherules found in Belize and Mexico and intense sulfuric acid rain in North America (see text).

impacts, but as noted above such impacts can result in >80% loss of the projectile mass to space (Vickery and Melosh, 1990). The estimates of meteoritic material retained by Earth in the K/T boundary provided by Kyte et al. (1985) can be used to place bounds on the possible volatile contribution of the projectile. Such estimates are presented in Table 2.

The most probable impact angle is 45°. Schultz and D'Hondt (1996) have argued that the Chicxulub impact was highly oblique, perhaps 20-30° from the horizontal. Schultz (1996) suggests that for a 15-30° oblique impact into a carbonate target, 15-20 times more vapor is produced than would be in a vertical impact. Most of this vapor comes from near-surface frictional heating; hence such estimates may well apply to sediments at Chicxulub. Nevertheless, there is some question as to the applicability of the relatively low velocity experiments ($\leq$6 km/s), upon which Schultz's estimates are based, to actual asteroid or comet impacts (Melosh 1989, p. 21). This is largely due to the greater coupling of energy to Earth's surface at high velocities. Furthermore, since sulfates vaporize at higher pressures and temperatures than do carbonates, perhaps the factor of 15-20 increase does not apply directly to sulfate vapor production.

Another important effect of an oblique impact, discussed by Schultz (1996), is that while the volume of the vapor plume may be larger in oblique compared to vertical impacts, the energy content of the plume is less resulting in a cooler plume. Therefore oblique impacts may produce more vapor, but much of this vapor may condense rapidly and not be globally distributed. This is especially true for sulfur oxides, which may condense as sulfate ($CaSO_4$ or H_2SO_4). This implies that highly oblique impacts may not greatly increase globally distributed CO_2, SO_2, and H_2O in the stratosphere compared to near-vertical impacts.

A simpler approach to estimating the effects of an oblique impact is to calculate the increase in the volume of sediments within the impact footprint. The volume of the footprint increases by a factor of 1/sin (vertical impact 90°). Thus the 1/sin factor provides a reasonable minimum for the increase in the amount of vaporized sediment in the hot fireball. For an impact angle of 45°, an increase of 40% is indicated. For the 30° impact suggested by Schultz and D'Hondt (1996), the volume of vaporized sediment would double.

Given the range of volatile masses in Tables 1 and 2 and the potential increases in the target volatile mass due to oblique impact, the maximum and minimum values for SO_2, CO_2, and H_2O ejected into the stratosphere and distributed globally by the Chicxulub impact cover a wide range. For our baseline estimates of the globally distributed stratospheric volatiles presented in Table 3, we selected parameters that produce volatile masses toward the low end of the range of reasonable values. We selected an asteroid and a comet with the mass and velocity required to create a D_f of 230-260 km. The size of these projectiles falls within the lower 1/3 of the range of possible values for either asteroids or comets. We assume (1) an oblique impact that caused a 100% increase in the hot fireball volatile mass given in Table 1 (increase due to footprint volume in a 30° impact); (2) no increase in the mass of the warm fireball due to the obliquity of the impact, since much of these cooler volatiles may not be globally distributed; (3) 30% of the warm fireball (out-of-footprint vapor) is globally distributed in the stratosphere (as SO_2, CO_2, and H_2O vapor) based on the laser experiments discussed by Ivanov et al. (1996); and (4) a projectile with typical S, C, and H_2O contents and complete vaporization upon impact. The projectile mass retained on Earth (from which the meteoritic vapor mass was derived) was calculated based on the size and density parameters given in Table 3 and a 40% asteroid retention and 30% comet retention (Vickery and Melosh, 1990). These meteoritic vapor masses fall in the middle to lower end of the possible ranges given in Table 2.

Table 2. Meteoritic Volatile Mass Injected Into Atmosphere

Projectile Mass Retained, Gt (10^{15} g)	SO_2 Gt (10^{15} g) Asteroid/Comet		CO_2 Gt (10^{15} g) Asteroid/Comet*		H_2O Gt (10^{15} g) Asteroid		Comet	
	6% S	2% S	3% C	0.5% C	17% H_2O	1% H_2O	50% H_2O	25% H_2O
450	54	18	50	8	77	5	450	225
980	118	39	108	18	167	10	980	490

Assumes all the meteoritic S and C in the retained mass are converted to SO_2 and CO_2 and that the water in comets is vaporized and retained in the same proportion as present in the projectile. S, C, and asteroid H_2O percentages based on nonvolatile component and represent the maximum and typical values for asteroids and comets. Projectile masses are the minimum (450 Gt) and maximum (980 Gt) values of nonvolatile meteoritic mass retained on Earth given by Kyte et al. [1985].

*Maximum C in an asteroid is about 3%, which is also typical of a 50% ice comet. A typical asteroid has about 0.5% C. No maximum C value for comets is given.

Table 3. Baseline Volatile Mass Globally Distributed in Stratosphere

	Projectile		SO_2				CO_2				H_2O			
	Diameter,	Velocity,	Gt (10^{15} g)				Gt (10^{15} g)				Gt (10^{15} g)			
	km	km/s	F	OF	P	Total	F	OF	P	Total	F	OF	P	Total
Baseline asteroid†	12	28	280	10	36	326	475	33	17	525	96	120	9	225
Baseline comet‡	16	28	495	13	19	527	833	40	53	927	167	120	480	767

Values based on calculations in Tables 1 and 2 with the modifications noted below. F, vapors from footprint, increased 100% due to oblique impact; OF, vapors from out-of-footprint interpolated from calculations in Table 1, assumes only 30% globally distributed in stratosphere; P, vapors from projectile, based on retained mass of 900 Gt for the asteroid (40% retention) and 480 Gt for the nonvolatile fraction of the comet (total mass 960 Gt, 30% retention).

†Asteroid density 2.5 g/cm^3; 2% S, 0.5% C, 1% H_2O.

‡Comet density 1.5 g/cm^3; 2% S, 3% C, 50% H_2O (S and C percentages based on nonvolatile fraction).

CLIMATE EFFECTS

Atmospheric Modeling

Our previous analysis (Pope et al., 1994) of the atmospheric effects of the injection of a large mass of vaporized sulfate into the stratosphere focused on two scenarios: (1) the rapid production of sulfuric acid aerosols, primarily from the warm fireball, and (2) the slow production of sulfuric acid aerosols involving the time-limiting photochemical oxidation of SO_2 from the hot fireball. Our atmospheric modeling contains three parts: (1) a radiative transfer model (Baines and Smith, 1990; Baines and Hammel, 1994); (2) a microphysical model of particle coagulation and sedimentation adapted from Toon et al. (1982); and (3) a SO_2 to H_2SO_4 conversion and stratospheric diffusion model adapted from Pinto et al. (1989) and empirical data. The conversion rate of stratospheric reservoir gases produced by the Chicxulub impact into sulfate aerosols can be estimated by extrapolating the model results of Pinto et al. (1989), originally developed for volcanic injections of SO_2 (Figure 4).

Figure 5 shows our model parameters for the sulfate aerosol distribution within the stratosphere at the conclusion of the first year of the scenario 2 model (initial SO_2 reservoir 200 Gt). The sulfate mass is nearly constant in each layer, as the aerosol formation rate varies by only 15% during the year. In contrast, the aerosol particle number density decreases by nearly 2 orders of magnitude from top to bottom, reflecting the quadrupling of particle radius due to coagulation.

Our discussion of the evolution of the warm fireball presented above emphasizes the need to consider that a significant portion of the vaporized sulfates may rapidly combine with abundant water and form sulfuric acid aerosols either in the plume or soon after dispersal: our scenario 1. We suggest that as much as 70% of the vaporized sulfur in the warm fireball may condense as H_2SO_4 during the initial injection and dispersion in the atmosphere. This indicates that about 20-30 Gt of SO_2 may convert to aerosol in the first few hours to days after impact. Much of this acid would probably rain out rapidly, but presumably a portion would be widely distributed, perhaps globally.

The major global atmospheric effects of the impact vaporized sulfates come from the long-term conversion of SO_2 and water vapor from the hot fireball into sulfuric acid aerosols. Our baseline calculations indicate that the Chicxulub hot fireball produced a globally distributed stratospheric reservoir with 326-527 Gt of SO_2 and 225-767 Gt of H_2O vapor (Table 3). Figure 6 shows the evolution of our nominal impact-generated stratospheric reservoirs of SO_2 and H_2O, here taken to be 200 Gt each. The water mass is the limiting factor because approximately equal amounts of SO_2 and H_2O are needed to produce aerosol (see below); hence we chose 200 Gt as our baseline mass for both SO_2 and H_2O. Figure 6 is derived from the coupling of the SO_2 conversion, diffusion, coagulation, and sedimentation components of our model.

Applying our radiative transfer model to the baseline volatile estimates, we find that the transmission of sunlight to Earth's surface (relative to pre-impact conditions) drops significantly for over a decade due to the formation of sulfate aerosols (Figure 7). These aerosols decrease the transmission by about ~80-90% in the year following the impact and remains more than 50% below normal for ~9 years for the 200 Gt case and ~13 years for the 2,000 Gt case.

Sulfate Cooling

The long-term reduction in solar transmission due to sulfuric acid aerosols (Figure 7) caused a major drop in global temperatures. If we apply the minimum 15 year timescale for the atmosphere-

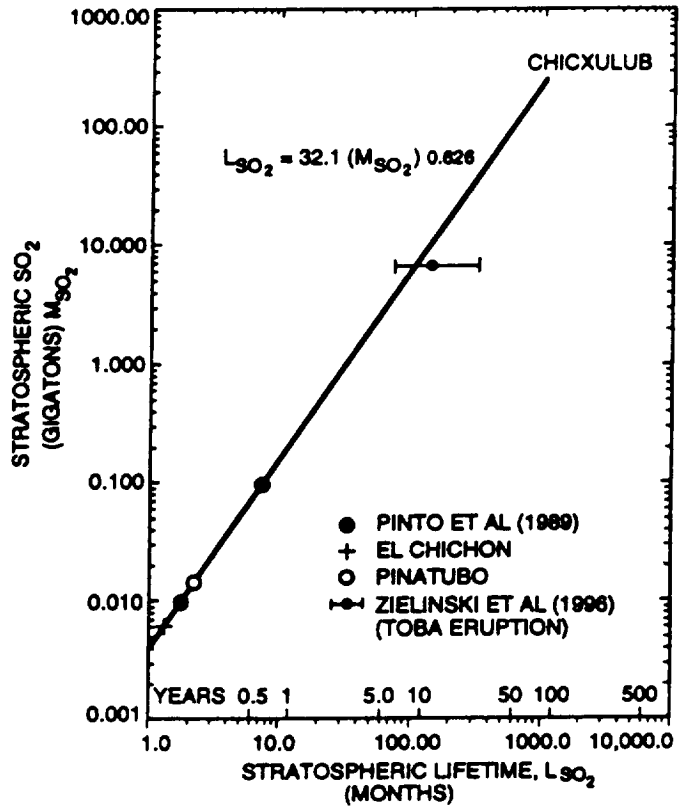

Figure 4. Instantaneous lifetime of stratospheric SO_2 (Lso_2) as a function of the initial mass loading of SO_2 (Mso_2). Power function based on a regression of lifetime values for 0.01 Gt (1.8 months) and 0.1 Gt (7.6 months) loadings calculated by Pinto et al. (1989). The Pinto et al. (1989) model agrees well with the observed lifetimes for the El Chichon and Pinatubo volcanic eruptions. Mso_2 and Lso_2 for El Chichon are those cited by Pinto et al. (1989) from Mroz et al. (1983) and Heath et al. (1983). Mso_2 and Lso_2 for Pinatubo are the best fit data points cited by Hoff (1992). Other values for these volcanic eruptions have been cited, reflecting uncertainties of about a factor of 2 for both Mso_2 and Lso_2. The power law extrapolation agrees well with our calculated lifetime (8.7 years) for the Toba eruption derived from the duration of sulfuric acid deposition recorded in the Greenland ice core (Zielinski et al., 1996). Lifetimes (with error bars) for the Toba 6.6 Gt loading of SO_2 are calculated by inverting our model of coagulation and sedimentation to fit the 6 ± 1.5 years of acid deposition noted by Zielinski et al. (1996).

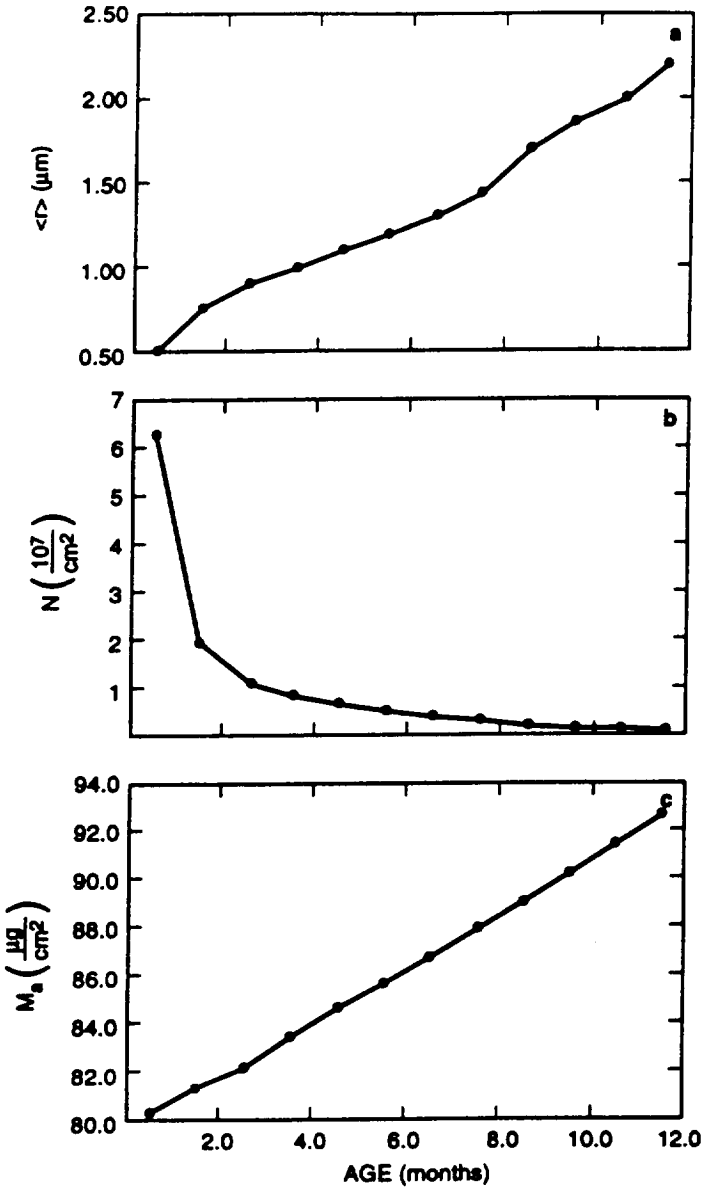

Figure 5. Model of global stratospheric aerosol (H_2SO_4:$2H_2O$) characteristics 1 year after impact for a nominal 200 Gt loading of SO_2 and H_2O. Graphs depict (a) mean particle radius, (b) column number density, and (c) column aerosol mass density for each of the 12 layers in the model (represented by dots on curves). Each model layer corresponds to a mean age in months after impact. Thus 1 year after impact, the first aerosol layer that formed has fallen to the lowest layer in the stratosphere (base at 10 km) and has a mean age of 11.5 months. Similarly, the last layer to form is at the top (30 km) and has a mean age of 0.5 months. Note the increasing mean particle radius (Figure 5a) and decreasing number density (Figure 5b) with age due to coagulation. Also note that the mass of aerosol formed (Figure 5c) gradually decreases over time (older layers have more mass) due to the shrinking size of the SO_2 reservoir as it is depleted by diffusion. The total column mass density at the end of the first year is 1035 microns/cm^2, which is equivalent to a conversion of about 2.5 Gt of SO_2 to acid aerosol.

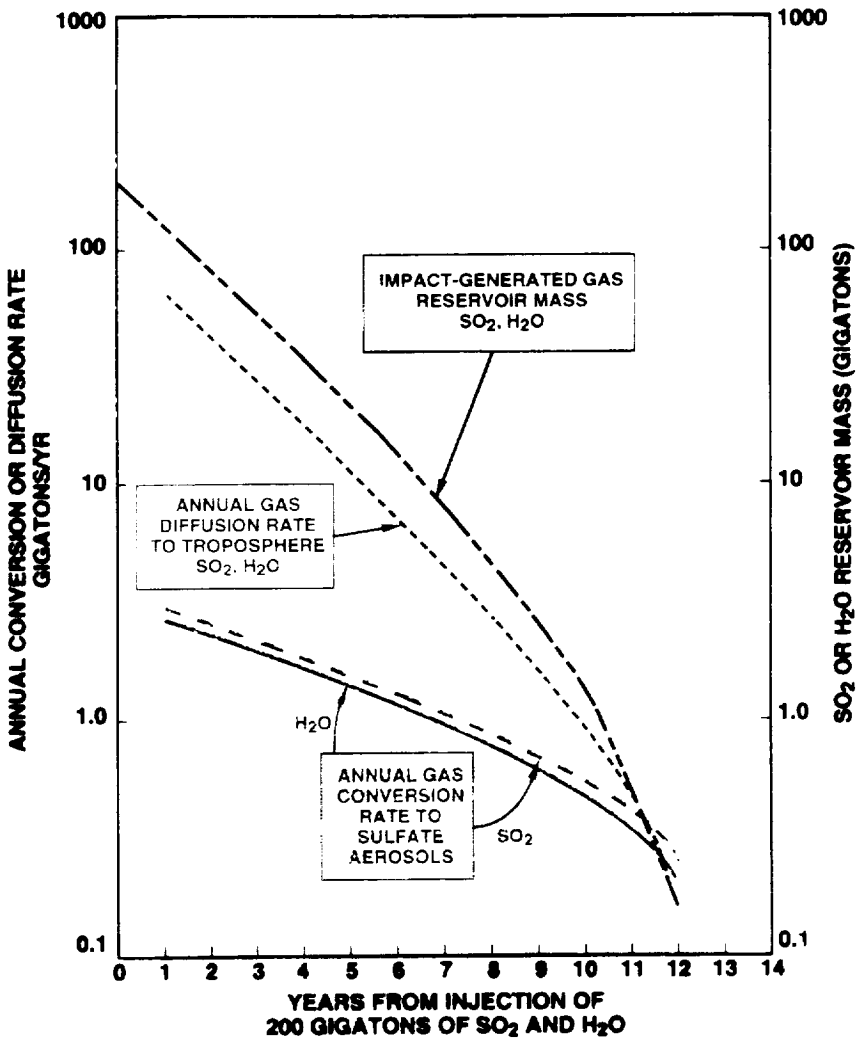

Figure 6. Evolution of the stratospheric SO_2 and H_2O impact-generated reservoirs. Reservoir masses (upper solid curve and right-hand scale) are shown as a function of time for an initial loading of 200 Gt each of SO_2 and H_2O (for simplicity, the SO_2/H_2O mass ratio for aerosol formation is shown as 1; actual ratios are 1.02-1.19). The upper dashed curve and left-hand scale give the annual diffusion rates for SO_2 and H_2O. The lower solid and dashed curves and left-hand scale give the annual rate of conversion of SO_2 and H_2O to sulfate aerosol. These curves demonstrate that diffusion is a much greater sink than conversion to aerosol until about the beginning of last year. For a 200 Gt loading, sulfate aerosol production lasts about 12 years (note that aerosol loading will remain high for about 1 year after production ceases).

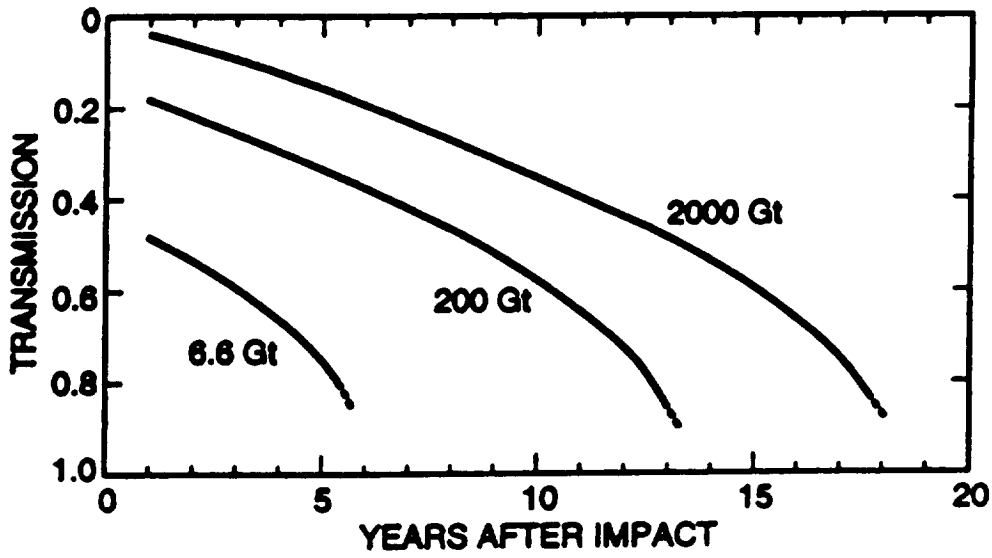

Figure 7. Solar transmission (wavelength 0.5 microns) following the Chicxulub impact. Postimpact transmission, relative to preimpact, is shown as a function of time for three cases: 6.6 Gt (Toba volcanic eruption), 200 Gt (Chicxulub baseline estimate), and 2000 Gt loadings of SO_2. Transmission evaluated using the vertically inhomogeneous aerosol model structure in Figure 5 and the stratospheric aerosol evolution shown in Figure 7.

ocean response proposed by Pollack et al. (1993) to our nominal 200 Gt case (transmission history in Figure 7) and assume that ambient temperatures just prior to impact were the same as today's (global average of 288°K), then the global average surface temperature would have dropped below freezing within 3 years and remained below freezing for nearly 20 years. The maximum average surface temperature drop would be ~31°K, which would occur near the end of the 10th year. By contrast, if we assume the same initial temperature, but the maximum 150 year timescale proposed by Pollack et al. (1993), then the global average surface temperature would drop only ~5°K after 13 years but would take over 100 years to return to preimpact temperatures. For comparison, our calculations for one of the largest volcanic eruptions recorded, the release of 6.6 Gt of SO_2 by the Toba eruption (Rose and Chesner, 1990; Rampino and Self, 1992), predict a 9.5°K cooling after 5 years for the 15 year timescale and about 1°K for the 150 year timescale.

GEOLOGICAL EVIDENCE FOR SULFURIC ACID AEROSOLS AT THE K/T BOUNDARY

Sulfate Vaporization

About 2-6% of the impact glass droplets produced by the Chicxulub impact and found in the K/T boundary are composed of a Ca- and S-rich yellow glass, which is best explained by an impact into a sulfate target (Bohor and Glass, 1995; Izett, 1991; Sigurdsson et al., 1991a, b, 1992). Analyses of sulfur isotopes and major and minor elements in these yellow glasses suggest that the melting that produced them released about 18% SO_2 (by weight) (Chaussidon et al., 1996). The mass of yellow glass in the K/T boundary is estimated at about 50 Gt (Sigurdsson et al., 1991b), which indicates that about 9 Gt of SO_2 were released by the melt.

The impact yellow glass was probably ejected with the warm fireball, as it is found in the basal ejecta layer beneath the debris associated with the hot fireball (Alvarez et al., 1995), and because most of the silicates would be vaporized in the hot fireball. The 9 Gt value is close to our baseline estimates of the globally distributed SO_2 in the warm fireball (10-13 Gt) (Table 1). Chaussidon et al. (1996) estimate that only about 2.6% (by weight) CO_2, or 1.3 Gt, was released by the yellow glass, which is more than an order of magnitude less than our estimates of globally distributed CO_2 in the warm fireball (33-40 Gt). This discrepancy may be explained by the sequestering of carbonates in the formation of carbonate spherules, which are also found in the basal ejecta layers in Belize (Ocampo et al., 1996a) and Mexico (Smit et al., 1996). These impact glass studies clearly indicate a massive release of SO_2 to the atmosphere, since the 9 Gt represents a minimum and probably does not reflect SO_2 in the hot fireball.

Sulfuric Acid Rain

Given that a massive release of SO_2 is fairly certain, the more critical uncertainties lie in our estimates of acid aerosol conversion. Our scenario 1 of rapid conversion of the warm fireball to aerosol remains speculative, and the chemical and physical dynamics of the warm fireball need to be studied further. Our long-term acid conversion rates depend upon the power law relationship we derived from empirical data and models of volcanic eruptions, which cover SO_2 loadings extending over 3 orders of magnitude: 0.005 Gt (El Chichon) to 6.6 Gt (Toba). Thus extension of this rate another 1.5 orders of magnitude (200 Gt) is not unreasonable.

Support for our two-phase scenario with rapid acid conversion in the warm fireball followed

by a second pulse of acid production comes from recent studies of acid leaching of K/T boundary ejecta and soils in eastern Montana (Retallack, 1996). Retallack found that the boundary bed, deposited in a matter of minutes after impact, was more leached than the overlying impact bed (also heavily leached), deposited over a period of months as the fine dust deposited on top of the stratosphere settled to the ground (e.g., Alvarez et al., 1995; Pollastro and Bohor, 1993). This pattern can be explained by our proposed two-part scenario, where leaching of the boundary bed occurred within hours to days due to rapid acid production and fallout from the warm fireball, followed by a second, prolonged period of acid deposition during the decade or more of acid rain caused by conversion of SO_2 from the hot fireball. Given this two-phase scenario, the boundary bed would be more heavily leached because it received two doses of acid rain compared to one for the impact bed. It is interesting to note that the eastern Montana sites studied by Retallack lie about 3000 km directly down range along the oblique trajectory proposed by Schultz and D'Hondt (1996). As noted above, a highly oblique impact may result in a cooler plume and more acid rain in the down range region.

Retallack (1996) calculates that the boundary bed received a minimum of 5.4 keq/ha more acid than the impact bed. Given our two-part scenario outlined above, this corresponds to an SO_2 equivalent mass of about 8.5 Gt for the warm fireball, calculated on a global basis. While this mass is remarkably close to that derived from the impact glass studies, it too is only a minimum. Retallack also estimates the upper limit to acid leaching, calculations made difficult by uncertainties related to the composition and bulk density of the ejecta layers prior to leaching. Assuming a parent material composition similar to the K/T tektites from Haiti, about 648 keq/ha of acid was consumed by the boundary bed and 319 keq/ha by the impact bed (assuming other parent materials reduces these estimates by a factor of 2) (Retallack, 1996). If we assume that this boundary bed leaching represents the total acid rain, then a total mass of 1000 Gt of SO_2 was converted to acid rain. Following this same assumption, the first and second pulse of acid resulted from the conversion of about 500 Gt each of SO_2. This assumes that both pulses were global; thus, if the warm fireball distribution was more regional, the total amount of SO_2 converted would be proportionally less.

The conversion of 500 Gt of SO_2 from the globally distributed hot fireball to sulfuric acid is consistent with our baseline calculations only if most of the impact-produced SO_2 was converted to acid. Our baseline calculations for stratospheric conversion of SO_2 to acid is only about 15 Gt, with the remaining 185 Gt diffusing to the troposphere as SO_2. Anthropogenic emissions of SO_2 into the troposphere are known to form tropospheric sulfuric acid aerosols (e.g., Charlson et al., 1992). Thus, Retallack's calculations are consistent with ours if the SO_2 that diffused to the troposphere was also converted to sulfuric acid rain. In our calculations of global cooling we neglected the cooling effects of any tropospheric sulfuric acid aerosols, which can be significant (Charlson et al., 1992). This again implies that our sulfate aerosol loading estimates are probably very conservative.

Additional evidence for sulfuric acid aerosol production by the Chicxulub impact comes from the marine $^{87}Sr/^{86}86$ record, which is characterized by an abrupt increase at the K/T boundary. This increase has been attributed to continental leaching caused by a brief, intense episode of acid rain (Macdougall, 1988; Martin and Macdougall, 1991). These studies indicate that the acid rain event was indeed global. Arguments have been advanced that the acid rain may be the result of nitric acid produced by shock heating of the atmosphere (Prinn and Fegley, 1987). Nevertheless, Zahnle (1990) has shown that for a Chicxulub-size event, only 10^{14} to 10^{15} moles of nitric acid would be produced, which is not sufficient to explain either the global Sr leaching or the ejecta leaching in Montana.

Global Cooling and Disruption of Ocean Circulation

Our radiative transfer calculations (Figure 7) of the effects of the long-lived aerosol are also conservative. We neglect transmission reductions resulting from impurities in the aerosols, non-aerosol gases, dust, or smoke, as well as from the tropospheric aerosols mentioned above. All these factors would decrease sunlight transmission over that estimated in Figure 7.

Future work will help refine our estimates of aerosol loading and solar transmission reduction, but significant uncertainties will remain in estimating temperature changes. Temperature estimates are difficult to make largely due to uncertainties in the amount of ocean cooling involved. Geological studies and global climate modeling are needed to help constrain the magnitude of ocean buffering of surface temperature reductions under massive sulfate aerosol loading.

Our calculations constrain the drop in the average surface temperature to between 5° and 31°K, with the true value perhaps near freezing (~15°). It is important to note that the recovery time from such a global temperature perturbation is also a function of the e-fold response time of the ocean-atmosphere system. Therefore, while climatic recovery from the 31°K cooling predicted from a 15 year e-fold response is about 20 years, the recovery from a 5° cooling from a 150 year e-fold time would take over a century. There is ample oxygen isotope evidence for a brief, 3-6° C cooling of surface and deep ocean water at the K/T boundary, but the data are sometimes contradictory and do not have sufficient temporal resolution to confirm our cooling predictions (see summaries by Sigurdsson et al. (1992) and by Cornfield (1994)). Perhaps the best terrestrial record is found in the paleobotanical data from North Dakota, which indicate a ~7°C temperature drop in the earliest Paleocene (10 cm above the K/T boundary) and the replacement of the local Cretaceous flora with cold-adapted, high-latitude species (Johnson and Wilf, 1996).

Given the massive sulfate loading of the atmosphere, the upper mixed layer of the oceans must have cooled dramatically, thus causing upwelling of deep ocean waters. Geological evidence for this perturbation is found in the marine delta ^{13}C record. In a stable, stratified ocean, ^{12}C is depleted and ^{13}C is enriched in the upper mixed layer due to the preferential use of ^{12}C in photosynthesis. Bottom waters have much lighter delta ^{13}C values because they are enriched in ^{12}C due to the respiration of light organic matter. This pattern results in a notable ^{13}C gradient between surface and bottom waters. Comparison of carbon isotopic values between surface and bottom dwelling organisms that produce calcareous shells confirms the presence of this gradient in the Late Cretaceous. This gradient collapses at the K/T boundary. This collapse has been one of the major arguments for the termination of photosynthesis at the K/T boundary and the development of a respiring "strangelove" ocean (e.g., Hsu and McKenzie, 1985, 1990; Zachos et al., 1989); however, the collapse may simply reflect a dramatic increase in global mixing of surface and deep waters caused by sulfate cooling of the surface. In fact, Zachos et al. (1989) suggested the collapse of this gradient could be from either a major drop in primary productivity or a change to extremely rapid rates of oceanic turnover. The oxygen isotope changes at the K/T boundary noted above are consistent with the latter view, indicating cooling of both surface and bottom waters and a disruption in circulation. Plankton blooms in the earliest Paleocene independently suggest a dramatic increase in upwelling at the K/T boundary (Hollis et al., 1995), a subject worth future study.

The impact-induced drop in solar radiation, and its effect upon ocean circulation, may have also led to a switch in bottom-water origin from tropical in the Cretaceous to polar in the early Paleocene. Switching was due to the increase in surface cooling at high latitudes and decrease in solar evaporation at low latitudes. This shift from a "greenhouse" to "icehouse" circulation pattern

may be reflected in the Milankovitch cycles found in pelagic sediments of the South Atlantic, Spain, and Italy. These sections show an abrupt change at the K/T boundary from precession-eccentricity dominated cyclicity to obliquity dominated cycles lasting about 1 Myr.

ANALYSES OF CHICXULUB IMPACT EJECTA FROM ALBION ISLAND, BELIZE

An enigmatic sedimentary deposit, now known as the Albion Formation, (Ocampo et al., 1996a) is exposed in a quarry on Albion Island located in the Hondo River of northern Belize, approximately 360 km southeast of the center of the Chicxulub impact crater (Figure 8). The deposit unconformably overlies dolomitized limestone of the Barton Creek Formation and is composed of a lower Spheroid Bed and an upper Diamictite Bed. Sedimentologic and petrographic evidence suggests that the Albion Formation is proximal ejecta from the Chicxulub impact crater (Ocampo et al., 1996a). The Albion Island exposure of ejecta is the closest yet found to the Chicxulub crater and is the only known surface exposure of the Chicxulub ejecta blanket with the possible exception of the recently discovered ejecta deposits in central Belize (e.g. Ocampo et al., 1996b, 1997). This paper presents several new observations that help confirm an impact origin for the Albion Formation and proposes an interpretation of the ejecta origin and depositional processes.

Barton Creek Formation

The Barton Creek Formation on Albion Island is composed of a buff-colored, 26-m-thick sequence of dolomitized limestone deposited in a shallow-water platform environment (Figure 8). Petrographic analyses indicate interbedding of shallow subtidal and intertidal sediments, some with nodular molds suggesting periodic emergence and evaporite deposition. Cathodoluminesence (CL) petrography indicates a complex paragenetic sequence of calcite cementation and dolomitization (Fouke et al., 1996a). Benthic foraminifera fossils are present in the section, but are too recrystallized to be identified. Nerineid gastropod fossils (Figure 9A) and a new species of fossil crab, *Carcineretes planetarius* (Vega et al., in press) (Figure 9B), are found near the base of the exposed section (Figure 81). Flores (1952) interpreted the Barton Creek Formation as representing a shallow, back-reef lagoon environment. This is consistent with the gastropods and crabs, as well as with the overall restricted fauna and lithology of the Albion quarry.

The Barton Creek Formation in central Belize contains Upper Cretaceous fossil rudistids, miliolids, rotalids, *Dyciclina* sp., *Lockhartia* sp., *Nummoloculina* sp., *Valvulina* sp. (Flores, 1952). The nerineid gastropods from Albion Island have infolding wall structures (Figure 9A) characteristic of the last developmental stage, indicating a Campanian to Maastrichtian age. Vega et al. (in press) tentatively propose a Maastrichtian age for the *Carcineretes planetarius* crabs found at Albion Island. The only other member of *Carcineretes*, *C. woolacotti,* comes from the early Maastrichtian (Morris, 1993).

$^{87}Sr/^{86}Sr$ isotope ratios (0.70786-0.70796) from Barton Creek Formation samples collected 2 m below the contact with the Spheroid Bed are consistent with, but do not confirm, a Maastrichtian age (Ocampo et al., 1996a). Five oriented samples of the Barton Creek Formation were analyzed for magnetic vectors (Figure 8). The four lower ones have normal NRMs, but the upper-most one is reversed, indicating a magnetic reversal 2.5 m below the contact with the Spheroid Bed. Several such paleomagnetic reversals occur in the Maastrichtian. The only one known in the Campanian occurs at the boundary with the Santonian: too early to fit the fossil evidence. The combined fossil, Sr isotope, and paleomagnetic data support a Maastrichtian age for the dolomitized limestone in the

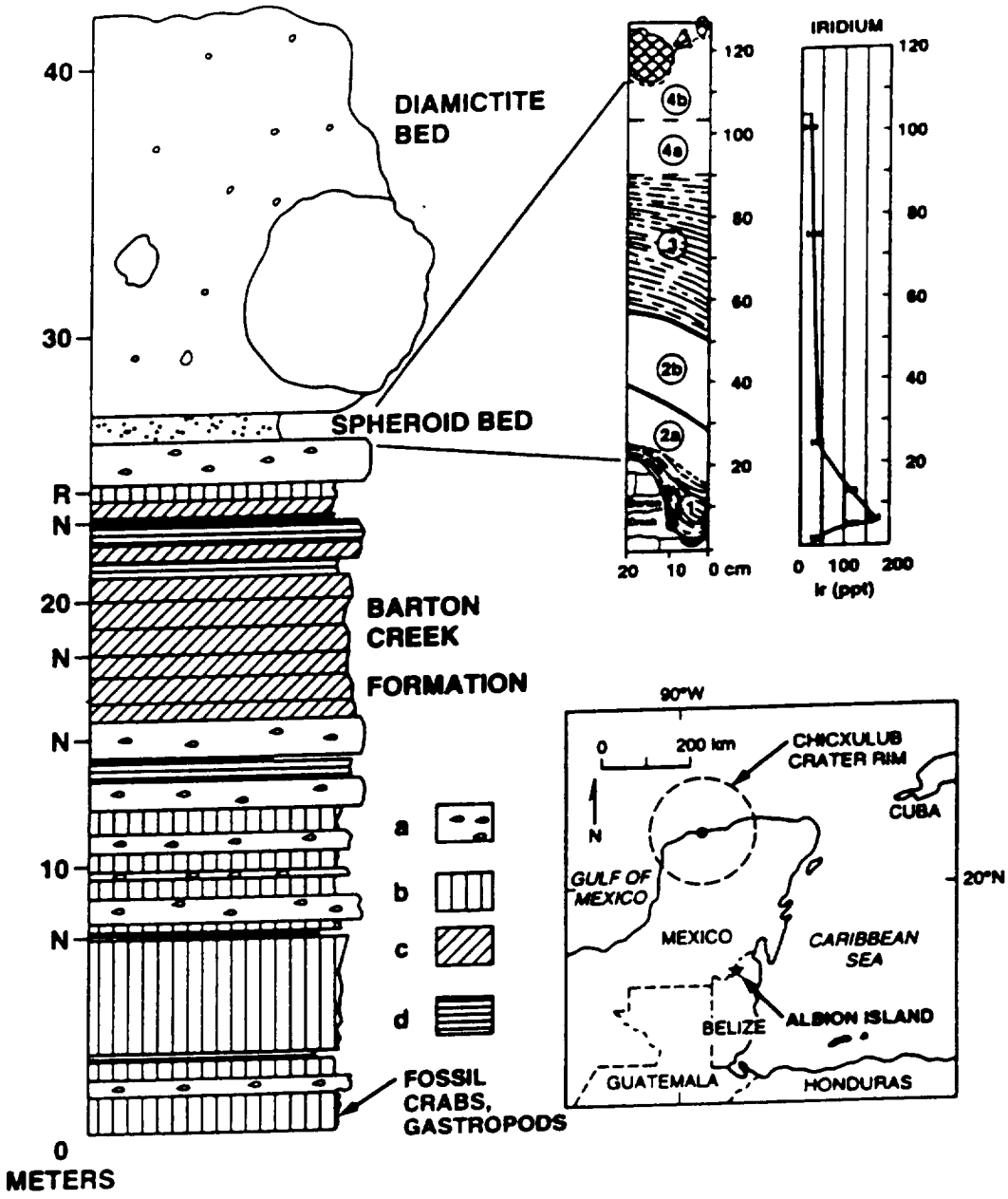

Figure 8. Composite stratigraphy of the Albion Island Quarry, northern Belize including detail of Spheroid Bed from the "Saddle" location. Spheroid Bed strata 1-4 are described in text, substrata (e.g. 2a, 2b) are local subdivisions not found in every quarry location. Note plot of Ir concentrations, locations of samples with normal (N) and reversed (R) paleomagnetism, and location of crab and gastropod fossils. Key to Barton Creek Formation dolomite: a) thick, coarsely crystalline beds containing vugs with the "chickenwire" structure suggestive of leached anhydrite nodules, b) thin, finely crystalline beds, c) crossbedded, coarse, calcarenite beds, and d) fine grained, organic-rich, laminated beds with hummocky and ripple crossbedding. Inset: Map showing the location of Albion Island and the buried Chicxulub impact crater.

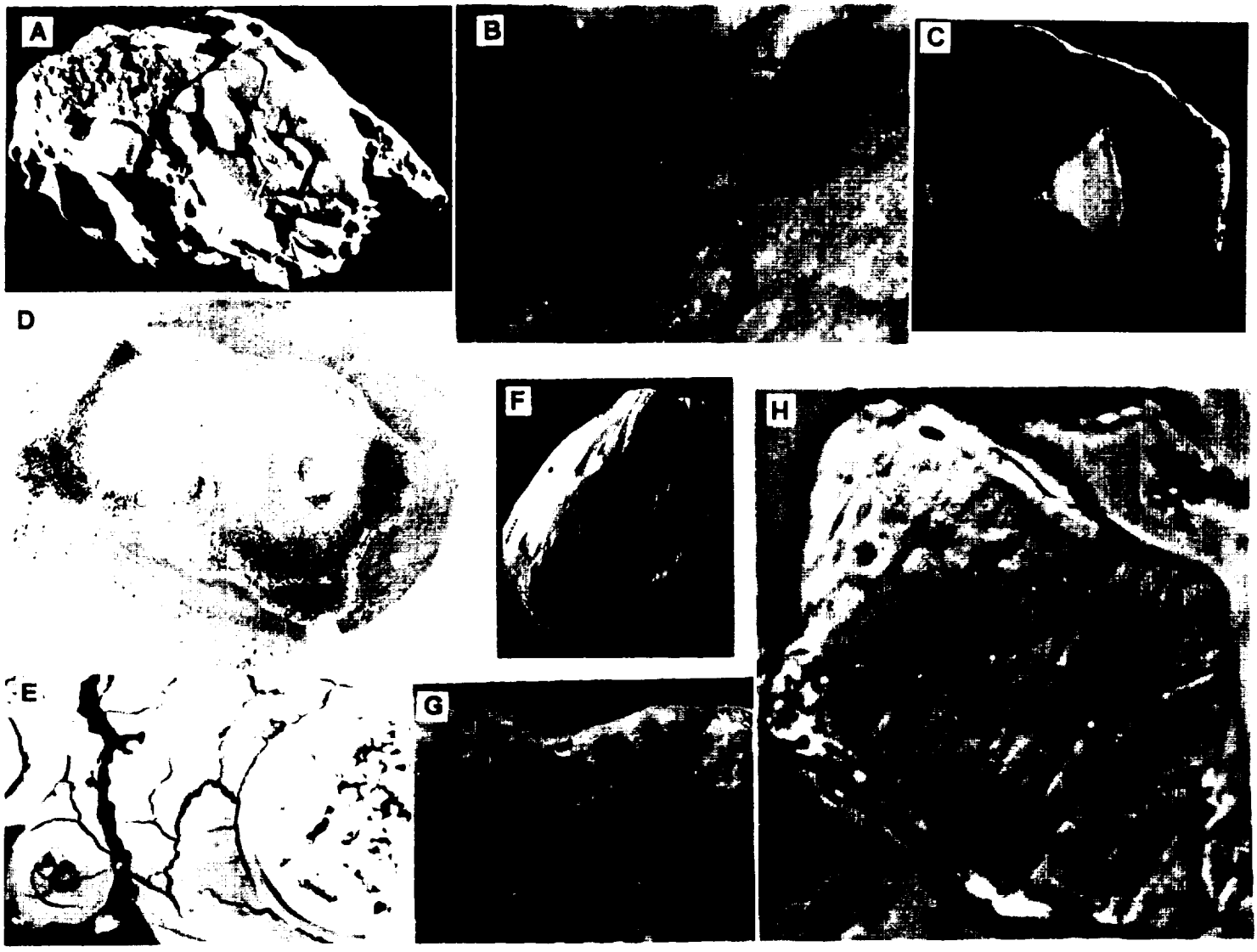

Figure 9. (A) Nerineid gastropod (mold width 1 cm) and (B) *Carcineretes planetarius* crab (carapace 5 cm wide) from Barton Creek Formation. Concentric dolomite spheroids (lapilli), (C) with an angular core (spheroid maximum width 1.8 cm) and (D) with two joined spheroidal cores (spheroid maximum width 2.5 cm), Albion Formation Spheroid Bed. (E) SEM image of a polished section of a palagonite fragment from a green clay spheroid showing relict a vesical (right) and spherulitic devitrification features (lower left) (field of view width 270 um), Albion Formation Spheroid Bed. (F) Striated dolomite cobble (height 10 cm) with close-up (G) showing penetrating lithic fragment (scale bar 1 cm), Albion Formation Diamictite Bed. (H) Shocked quartz grain showing two possible sets of planar deformation features (maximum width 100 um), Albion Formation Diamictite Bed.

Albion Island quarry.

The Barton Creek Formation in the quarry was folded into a gently plunging anticline, the apex of which was eroded prior to deposition of the overlying Albion Formation. The upper surface of the Barton Creek Formation is irregular with local abrupt relief of 20-50 cm. This surface contains preserved patches of a caliche cap (Figure 10), suggesting that Albion Island was emergent prior to the deposition of the Albion Formation. This caliche is composed of poorly sorted, angular fragments of the Barton Creek Formation dolomite re-cemented with micritic dolomite and coarse-grained calcite with iron oxide crusts and root casts. Such a surface is similar to the caliche caps found on emergent portions of the Pleistocene Yucatan platform (e.g. Ward, 1985) and emergent surfaces in other carbonate platform sequences (e.g. Fouke et al., 1996b).

Albion Formation Spheroid Bed

The Spheroid Bed unconformably overlies the Barton Creek Formation (Figure 8). It ranges in thickness from 0.10-1.72 m, but averages about 1 m in thickness. The lower contact is sharp. The upper contact is marked by the abrupt appearance of cobbles of the overlying Diamictite Bed, but with little change in the matrix. In most quarry locations the basal, and occasionally the upper, contact is a ~2-cm-thick brown clay layer with pronounced slickensides. Similar clay layers occur along shear plains that cut diagonally across the bed (Figure 8).

Four distinct strata with gradational contacts, numbered 1 at the base through 4 at the top, are differentiated based upon the presence and absence of certain clast types and foliation (Figure 8). All four strata contain 10-30% (by volume) dolomite spheroids 1-10 mm in diameter and 10% (by volume) flakes and angular clasts of brown clay 1-3 mm in diameter. Spheroids are supported in a weakly consolidated, fine-grained dolomite and clay matrix. Rare dolomite spheroids reach sizes of 20-25 mm. Green clay spheroids 1-10 mm in diameter comprise 10-30% (by volume) of stratum 1 and grade upward into the base of stratum 2 (Figure 8). No size grading of spheroids is visible in outcrop.

Stratum 1 is orange to pink and ~15-20 cm thick. The dolomite and green clay spheroids are flattened and deposited with the long axis parallel to the underlying Barton Creek Formation surface giving the bed a foliated appearance that follows the microtopography. Stratum 2 is mottled white, orange, and pink, ~25-40 cm thick, and contains slightly flattened dolomite spheroids and has faint foliation. Stratum 3 is orange, ~40-50 cm thick, and contains spherical to slightly oblate dolomite spheroids, distinct foliation, and 10% (by volume) white, chalky, angular dolomite clasts in the same size distribution as the spheroids. Stratum 4 is mottled orange to pink, ~40-50 cm thick, and contains spherical to slightly oblate dolomite spheroids, no foliation, and ~10% (by volume) white, chalky, angular dolomite clasts in the same size distribution as the spheroids. This upper-most stratum is only present in Spheroid Bed sections >1 m thick and has apparently been eroded where absent.

The matrix of the Spheroid Bed is largely composed of sucrosic 25-50 um dolomite crystals with concentric red/yellow CL zonations, which contrast with the bright, concentric red/orange CL zonations in the dolomite crystals of the spheroids (Fouke et al., 1996a). The matrix also contains interstitial iron oxide and smectite. The smaller (<5 mm) dolomite spheroids are composed of crystals of uniform size (25-50 um). Spheroids >5 mm have more heterogeneous crystals sizes and many have concentric structures, most common of which are bands of iron oxide. Most spheroids in the 10-25 mm range show concentric bands of fine and coarse dolomite crystals and iron oxide staining surrounding an angular core (Figure 9C). One large spheroid contains a core composed of two

Figure 10. Albion Island quarry. Photograph showing the caliche surface at the top of Barton Creek Formation dolomite.

smaller spheroids joined together (Figure 9D). Coarse spheroid bands have crystal sizes up to 500 um, but most bands have 50-75 um crystals. The angular cores are composed of a white, chalky, very fine-grained (~10 um) dolomite that is similar to the white, chalky, angular dolomite fragments abundant in the upper strata of the Spheroid Bed.

The green clay spheroids at the base of the Spheroid Bed have a dull, waxy appearance. X-ray diffraction (XRD) analyses indicate they are mostly smectite. Petrographic and microprobe analyses reveal that portions of some spherules are isotropic and have Si/Al ratios (Table 4) higher than typical smectites, as found in other K/T boundary clay spherules (Bohor and Glass, 1995; Kring and Boyton, 1991). Scanning electron micrographs (SEM) and thin sections of the clay spheroids show vesicular and spherulitic textures typical of devitrified glass (Bard, 1986) (Figure 9E). Based on this textural, mineralogic, and chemical data, we interpret the clay spheroids as altered glass, in most part transformed into palagonite, a common alteration product of glass (e.g. Fisher and Schmincke, 1984: Chapter 12). The interstitial clays and brown clay clasts appear to lack spherulitic and vesicular textures. These clays may be more highly altered glass, or perhaps the alteration products of other silicate rocks, which would be unstable in such a carbonate-rich environment.

Microprobe analyses of major oxides indicate that the palagonites in the green clay spheroids are compositionally similar to the Haitian palagonites formed from K/T boundary glass spherules (Table 4) (Bohor and Glass, 1995; Koeberl and Sigurdsson, 1992). We performed instrument neutron activation analysis (INAA) of bulk samples from Spheroid Bed strata 1, 2a, 3, and 4a, as well as from the Barton Creek Formation contact with the Spheroid bed, the brown clay at the base of the Spheroid Bed, and from clay-rich masses in Diamictite Bed (Figure 8, Table 4). Variance in the trace element abundance indicates four groupings (Table 5), which closely follow the stratigraphy. A slightly elevated concentration of Ir occurs in stratum 1, the green clay spheroid layer. The INAA analysis and additional radiochemical neutron activation, X-ray fluorescence, and microprobe analyses detected no other anomalously high concentrations of siderophile elements. Ir/Fe ratios are similar throughout the sequence and there are large coherent variations in the abundance of Ir, Fe, Hf, Ta, and Sc, which are often carried or associated with clay. The abundance of these elements do not vary directly with clay content, which varies only a few percent between samples, and instead appears to be associated with the green clay spheroids, which only occur in strata 1 and 2a. Analyses of these clay spheroids indicate trace element abundances similar to the bulk samples, but with higher concentrations, including Ir and notably Co in one sample.

Albion Formation Diamictite Bed

The Diamictite Bed is 15 m thick and extends from the Spheroid Bed to the surface of the quarry (Figure 8). An erosion surface cuts the top of the Diamictite Bed and we found no deposits overlying it, therefore its original thickness is unknown. The diamictite is unstratified, poorly sorted, matrix supported, and contains primarily carbonate and clay clasts, although several other components are present in trace amounts. It is weakly consolidated except for the basal 10-30 cm, which is well indurated and weathers into large cobbles.

Carbonate clasts are angular to subrounded and range in size from sub-millimeter grains to boulders 7.5 m in diameter (Ocampo et al., 1996a). Clasts 20-30 cm in diameter and smaller are common, whereas larger clasts are rare. Most of the carbonate clasts are dolomitized limestone and the matrix is a micritic dolomite (10-60 um crystals) with minor amounts of interstitial clay and iron oxide. Multiple generations of CL-distinct dolomite cements are found in the matrix and in the

Table 4. Major oxide analyses from the Albion Formation and K/T boundary in Haiti.

	Spheroid Bed* Palagonite n = 12	Diamictite Bed* Palagonite n = 11	Spheroid Bed^ Bulk Sample n = 3	Haiti K/T Spherule* Palagonite n = 5
Na_2O	0.06±0.02	0.06±0.05	0.04±0.02	0.6±0.2
MgO	9.65±0.72	8.56±0.51	17.60±1.91	6.5±0.4
Al_2O_3	16.70±1.17	16.42±0.67	3.69±2.17	15.7±1.6
SiO_2	58.21±3.27	57.33±2.31	11.05±6.70	61.1±1.8
K_2O	0.36±0.07	2.00±1.06	0.13±0.14	0.2±0.1
CaO	0.13±0.22	0.13±0.04	24.33±4.35	0.7±0.1
TiO_2	0.65±1.13	0.93±0.78	0.17±0.09	0.5±0.2
MnO	0.02±0.01	0.01±0.01	<0.01	no data
FeO	3.43±0.50	6.02±2.09	1.53±0.49	7.6±1.0
L.O.I.			41.57±3.39	
Total	89.20±4.95	91.46±2.25	100.13±0.15	92.9±3.5

* Microprobe analyses of palagonite shards selected under electron backscatter imaging. Error is one standard deviation. Haiti K/T spherule analyses from Bohor and Glass (1995).

^ X-Ray Fluorescence Analyses of oven-dried bulk samples. L.O.I. = loss on ignition.

Table 5. Instrument Neutron Activation Analyses (INAA)

	Group IV		Group III			
	Barton Creek 95-9	Basal Clay 95-8a	Spheroid 1 95-7	Spheroid 1 95-7a	Spheroid 2a 95-10b	Haiti K/T Black glass
Ir	15+4	30+5	111+14	152+14	123+11	<2000+0
Ce	3.88+0.7	6.03+0.11	6.98+0.17	6.3+0.3	10.9+0.2	46.30+4.42
Co	1.18	7.25	1.17+0.02	6.84	1.45+0.02	14.77+0.97
Cr	---	0.8+0.7	9.9+1.8	4.6+2.0	5.3+1.7	27.43+2.48
Cs	0.157+0.009	0.239+0.009	1.65+0.03	1.34+0.02	0.724+0.033	1.57+0.34
Eu	0.087+0.001	0.147	0.067+0.001	0.044+0.001	0.142	1.52+0.12
Fe	0.392	0.391	3.77	4.16	2.620	4.64+0.18
Hf	0.317+0.006	0.321+0.006	4.46	4.55	3.45	4.06+0.38
Ni	6.8+1.4	11.1+1.9	10.1+5.1	21.1+4.7	14.9+3.7	22+13
Sb	0.946+0.016	0.746+0.018	2.24+0.07	3.53+0.06	2.97+0.05	0.28+0.07
Sc	1.099	1.454	15.88	15.72	11.53	20.59+0.79
Se	0.988	8.31	0.361+0.016	0.199+0.009	0.284+0.011	0.00+0.00
Ta	0.041+0.001	0.041+0.001	0.497	0.533	0.436	0.33+0.14
Th	0.34+0.03	0.35+0.06	1.90+0.08	2.43+0.15	2.09+0.11	6.36+0.72
Zn	9.3+0.6	5.5+0.6	42.1+2.1	62.7+1.7	37.3+2.1	27.1+11.5

Table 5. (cont) Instrument Neutron Activation Analyses (INAA)

	Group II			Group I		
	Spheroid 2b 95-11a	Spheroid 3 95-13	Spheroid 4a 95-14	Diamictite 95-19a	Diamictite 95-37	Haiti K/T yellow glass
Ir	40+7	29+9	21+8	27+18/14	8+18/8	2000+1000
Ce	9.3+0.1	9.6+0.1	11.9+0.1	6.8+0.3	6.5+0.3	35.83+5.07
Co	0.733+0.008	0.614+0.010	1.02	3.39	2.15	22.74+3.53
Cr	5.8+1.0	4.3+1.0	4.2+1.0	33.9+2.5	23.7+2.2	29.7+10.9
Cs	0.161+0.015	0.040+0.018	0.035+0.017	3.39+0.04	2.22+0.04	2.43+0.65
Eu	0.222	0.353	0.345	0.128+0.002	0.167+0.002	1.17+0.22
Fe	1.272	0.859	0.592	2.402	1.277	4.51+0.30
Hf	1.27	1.02	0.851+0.012	3.27+0.04	2.25+0.03	3.23+0.17
Ni	14.3+2.4	8.7+3.0	6.3+3.2	24.9+7.5	15.0+6.6	285+135
Sb	1.51+0.03	0.285+0.023	0.155+0.024	1.58+0.07	0.83+0.06	2.56+0.82
Sc	4.80	4.47	4.29	9.81	6.88	21.34+0.82
Se	0.278+0.008	0.514+0.10	1.04	0.101+0.019	0.095+0.017	2.63+1.39
Ta	0.159+0.002	0.086+0.002	0.080+0.002	0.463+0.005	0.309+0.004	0.66+0.25
Th	1.34+0.06	1.80+0.05	1.60+0.06	3.15+0.14	2.70+0.12	5.08+0.82
Zn	15.1+1.0	5.3+1.2	4.3+1.1	42.8+2.5	27.2+2.3	74.3+14.2

* Detection limit for each element given in parenthese (Belize samples only). All values are in ppm, except for Au and Ir, which are in ppb.
^INAA analyses of smectite shells (probably palagonite, cf. Bohor and Glass, 1995) on glass spherules, from Koeberl and Sigurdsson (1992).

carbonate clasts (Fouke et al., 1996a).

Rare carbonate clasts exhibit striations in a single or occasionally multiple directions and in many cases terminate in an abrupt angular surface (Figure 9F). These striations range from microscopic sets that grade into a fine polish, to parallel grooves 1-2 mm deep. Sand-sized carbonate grains occur within some striae. In one sample a dolomite rock chip penetrated the clast to form a pit with a striated wall (Figure 9G).

The clay clasts comprise about 10% (by weight) of the Diamictite Bed, determined from acid-leach residues. They range in size from <1 mm to 4 cm, but most are <1 cm in diameter. The clays are mostly green and upon exposure, weather dark red. Petrographic, XRD, and SEM analyses of the clays reveal they are smectite and palagonite. Many of the clay fragments have the same vesicular textures and spherulitic devitrification features found in the green clay spheroids of the Spheroid Bed and are also interpreted to be altered glass. Some of the clay fragments without spherulitic or vesicular textures may be altered silicate rock fragments. Compositionally, the palagonites of the Diamictite Bed are similar to those of the Spheroid Bed, except that the former contain slightly more K and Fe (Table 4).

Clay-rich masses 0.5-2 m in diameter and light green or orange in color are found in the diamictite. Thin section analysis reveals that they are similar to the diamictite dolomite matrix with only a few percent more clay. INAA data (Table 5) show elemental abundances typical of crustal rocks. These clay-rich masses rarely contain radially fibrous calcite spherules about 1 cm in diameter that occur individually or in amalgamated masses (formerly referred to as pisoids, Ocampo et al., 1996a). The surfaces of the spherules are rough and appear etched and commonly have wart like protrusions. Some of these calcite spherules have angular cores of dark gray dolomite. The calcite spherules have a homogeneous orange CL (Fouke et al., 1996a).

Petrographic analyses of authigenic quartz found within vugs in the Diamictite Bed reveal anhydrite inclusions in the quartz. These vugs may represent leached anhydrite clasts and the anhydrite inclusions may reflect anhydrite replacement by quartz. Acid leach residues from the diamictite contain gypsum as finely disseminated crystals. Sulfates were apparently once common in the Diamictite Bed, but have been mostly leached.

Several other rare lithologies, some currently represented by single clasts, are described in detail by Ocampo et al. (1996a). They include Early Cretaceous fossiliferous limestone, dark gray dolomite, mud balls, granitic rock fragments, and detrital quartz. We recently found a single detrital quartz grain in an acid leach residue of a 200 g sample of diamictite that has one prominent set and a second clear set of planar deformation features (Figure 9H), indicative of shock. Detrital quartz is rare and typical grain smears of >63 um insoluble residues produce only a few detrital quartz grains per slide (authogenic quartz is common).

Interpretations

The presence of altered glass, striated and impact-penetrated cobbles, shocked quartz, and possible meteoritic material (Ir anomaly) in the Albion Formation provide good evidence that it is of impact origin. Confirmation that the underlying carbonates are Late Cretaceous, possibly Maastrichtian, strengthens the association of the Albion Formation with the nearby K/T Chicxulub crater. Nevertheless, our interpretation of the Albion Formation as Chicxulub ejecta is not based upon the formation's coarse age resolution, but on its impact origin and proximity to Chicxulub. We find it highly unlikely that the coarse ejecta on Albion Island could come from some other,

undiscovered large impact on the Yucatan Platform.

The shallow-water (<30 m) depositional environment and caliche cap of the Barton Creek Formation indicates that little or no surficial water was present at Albion Island at the time of impact. This is a key factor, because the Belize ejecta represent deposits that have not been affected by settling or flow through a water column, in contrast with other proximal ejecta deposits (e.g. Grajales et al., 1996; Smit et al., 1996). This terrestrial depositional environment simplifies the application of models of ejecta emplacement and comparisons with extraterrestrial ejecta deposits.

The concentric dolomite spheroids are good carbonate analogues of the siliceous accretionary lapilli from volcanic pyroclastic deposits. Carbonate lapilli have been recently reported from other proximal Chicxulub deposits (Grajales et al., 1996; Smit et al., 1996). The origin of the Albion Formation spheroids is best explained by accretion in a volatile-rich, turbulent flow. The absence of graded beds argues against air fall. Stratification within the bed indicates that the composition of the turbulent flow evolved as it passed over Albion Island, first depositing glass and later angular carbonate clasts, while continuously depositing carbonate spheroids. The flattening of spheroids may indicate that they were soft when first deposited and the alternating zones of foliation may reflect fluctuating confining pressures of the air blast associated with the initial expansion of the vapor plume.

The slightly elevated Ir concentrations in the base of the Spheroid Bed may reflect jetting of meteoritic material. Nevertheless, if the bed contains jetted material it must be highly diluted, because impact models suggest a jet composition of 20-50% projectile (Vickery, 1993), which would produce at least 1000 times more Ir than we observe. The rather small absolute abundance of Ir, and its close association with Fe and the other elements noted, could indicate a terrestrial source, but if so, the mechanism by which the Ir was concentrated in the base of the Spheroid Bed is unclear. The relatively high Ir abundances are associated green clay spheroids, which have the highest Ir concentration measured, suggesting the Ir may have been contained in the melt. The source of such a melt is unknown since the impact melts at Chicxulub contain mostly minor amounts of Ir (Claeys et al. 1995; Rochia et al., 1994) and as we noted above melted projectile should have much more Ir. High Ir abundances (up to 13.5 ppb) have been reported from some Chicxulub impact melt samples and appear to reflect rare Ir metal nuggets (Schuraytz et al., 1994). These high Ir abundances are controversial however, because more extensive analyses of these melts have produced consistently <0.1 ppb Ir (Claeys et al., 1995; Rocchia et al., 1994). It is difficult to explain the broad peak of Ir enrichment at the base of the Spheroid Bed with such non-uniform dissemination of metal Ir nuggets. We conclude that this Ir enrichment may indicate a slight mixing of meteoritic material with the first ejecta, but this is not yet confirmed.

The penetrating rock chip found in one of the diamictite cobbles must have impacted when the cobble was "soft", as high velocity impacts between solid ejecta particles produce radial fractures and spallation zones (Prasad and Sudhakar, 1996), not the grooved penetrating features we observed. It is unlikely that this clast would have survived impact if it were soft carbonate mud at the time of impact, thus we interpret the plastic deformation as evidence for ejecta particle interaction under pressures (100-1000 bars) and temperatures (>1500° K) sufficient to partially melt carbonates (e.g. Tyburczy and Ahrens, 1986). Such pressures and temperatures may be reached during the initial ejection, or when the vapor plume passed through the ejecta curtain (Vickery, 1986).

The radially fibrous calcite spherules are texturally similar to calcite spherules found in meteorites. The etched surfaces and wart like protrusions on the Albion Formation calcite spherules

have also been noted on altered glass spherules from the K/T boundary and on unaltered microtektites (Izett, 1991). The clay-rich masses and calcite spherules in Diamictite Bed may derive from calcite-rich impact melt.

The Barton Creek Formation carbonates are composed of several size-distinct and CL-distinct generations of cement and replacement dolomite, which are different with respect to size and CL from the dolomites in either the Spheroid or Diamictite Beds. Furthermore, the dolomites in the Spheroid Bed are different in size, CL character, and composition from the dolomites comprising the matrix and allochthonous blocks of the Diamictite Bed. No evidence of dolomite cement overgrowths on detrital dolomite crystals or fragments was observed with CL in either the Spheroid or Diamictite Beds. These observations suggest that: 1) the fluids that dolomitized the Barton Creek Formation, Spheroid Bed, and Diamictite Bed were chemically distinct from one another; 2) the Barton Creek Formation limestone was dolomitized prior to deposition of the ejecta; and 3) neither the Spheroid Bed dolomites nor most of the dolomitized allochthonous blocks in the Diamictite Bed were derived from the directly underlying Barton Creek Formation (we did find one block with a *Carcineretes planetarius* fossil, suggesting at least some blocks may be from the Barton Creek Formation).

Comparisons with Ries Crater

Ocampo et al. (1996a) interpreted the Spheroid Bed as a deposit from the lateral blast of the vapor plume, which entrained the smaller ejecta as it blew through the ejecta curtain, and the Diamictite Bed as a product of ballistic sedimentation coupled with debris flow processes similar to processes that formed the Bunte breccia at Ries Crater in Germany. This scenario explains the two-part stratigraphy in Belize, which is reversed from that of the Ries crater. Ries has coarse Bunte breccia at the base overlain by melt-rich breccia (suevite) with spherules (chondrules) and lapilli (Graup, 1981).

The Bunte breccia extends two crater radii from the center of the Ries crater and Albion Island is about three crater radii from the center of the Chicxulub crater (assuming a radius of 130 km, Pope et al., 1996; Sharpton et al., 1996). This greater distance for Albion Island might explain the apparent inversion of stratigraphy. There may be a cross-over point between the ejection velocity and the angle of trajectory where low velocity coarse ejecta are deposited first near the rim, but arrive after the high velocity, high altitude ejecta at greater distances. This may especially be true if the coarse debris is deposited ballistically near the rim, and then evolves into a turbulent flow at greater distances.

Ballistic sedimentation is the proposed origin of the Bunte breccia at Ries, where the scarcity of deep target rocks is attributed to dilution by scoured local bedrock produced by secondary impacts (Horz et al., 1977, 1983). Such scouring is a possible origin for much of the debris in the Albion Formation Diamictite Bed, but our observations cannot confirm this. There is no evidence of significant erosion at the base of either the Spheroid or Diamictite Beds, although we have no way of determining if this is a local or regional condition. The CL analyses of the diamictite suggest little local material is present, but it could contain scoured debris transported latterly from a platform region closer to the crater with a distinctly different dolomitization history.

The polish and striations observed on cobbles of the Diamictite Bed have also been reported from carbonate clasts in the Bunte breccia, where they were attributed to abrasion during ground surface flow (Chao et al., 1978). For the Albion Diamictite Bed, we suggest that some and perhaps most of the striations, as well as the related penetration features, may have formed during ejection

or transport in the ejecta curtain. In summary, we cannot rule out the possibility that most of the Diamictite Bed is composed of primary ejecta from Chicxulub.

We now recognize an alternative hypotheses to ballistic sedimentation for the emplacement of the Diamictite Bed, which is a turbulent flow of primary ejecta produced by atmospheric drag on the advancing ejecta curtain (Barnouin-Jha and Schultz, 1996; Schultz and Gault, 1979, 1982). The paucity of basement silicate clasts at Albion Island can be explained by the dominance of carbonates and sulfates in the upper 2-3 km of the target (Ward et al., 1995), and that the high ejection velocities needed to reach Belize only occur at shallow target depths (Melosh, 1989:73).

Either ballistic sedimentation or a drag-induced turbulent flow may have formed the Diamictite Bed. We view the Albion Island deposit as a good analogue of the fluidized ejecta blankets found on Mars (e.g. Schultz and Gault, 1979). Thus future research in Belize may help determine the origin of these enigmatic ejecta deposits.

The apparent abundance of melt (altered glass) in the Albion Formation Diamictite Bed contrasts with the melt-poor Bunte breccia (Horz et al., 1977, 1983) and its equivalent on the Chicxulub crater rim (Sharpton et al., 1996). This may reflect the massive dispersal of impact melt by expanding vapors as proposed by Kieffer and Simonds (1980) for impacts into volatile-rich targets like Chicxulub. The vesicular nature of the Albion Formation altered glass supports this view. We conclude, as did Alvarez et al. (1995) for the distribution of shocked quartz, that many of the unusual features of the Albion Formation derive from the explosive release of vapors by the Chicxulub impact into the Yucatan carbonate platform.

ANALYSES OF CHICXULUB IMPACT EJECTA FROM CAYO DISTRICT, BELIZE

Deposits of coarse carbonate ejecta have been found at the K/T boundary in the Cayo District of central Belize (Figure 11), 475 km southeast of the Chicxulub crater (Ocampo et al., 1996b). Unusual carbonate clasts found in the ejecta include angular to rounded pebbles and cobbles that exhibit surface polish, striations, and penetration by impacting rock chips. These clasts have been found in three locations and are named Pook's Pebbles, after the type locality near Pook's Hill Lodge south of Teakettle (Figure 12). We propose that the phenomena on the Pook's Pebbles are the product of interactions between ejecta particles, the vapor plume, and the atmosphere during ejection from Chicxulub and atmospheric re-entry from high altitudes.

Striations, Penetration Features, and Polish

The striae range from a few microns in width to a few millimeters and usually occur in parallel sets (Figure 13). Some clasts have as many as three overlapping sets and in several examples sets of striations curve and jog giving a "wiped" appearance. Many sets of striations end in abrupt angular terminations or pits that rarely contain the rock chips that created the striations (Figure 14). Small craters (1 cm) with up-turned rims are also present (Figure 14).

The polish is remarkably fine giving many clasts a sparkling sheen (Figure 14). Scanning electron microscopy reveals that the polish is so fine that the crystal boundaries between 1 micron grains appear annealed (Figure 15). In most cases the polish occurred after the striations, although it tends not to remove the striations, but only smooths the edges. Many of the polished limestone clasts contain patches of coarse-grained calcite crusts that have been polished along with adjacent areas without crusts.

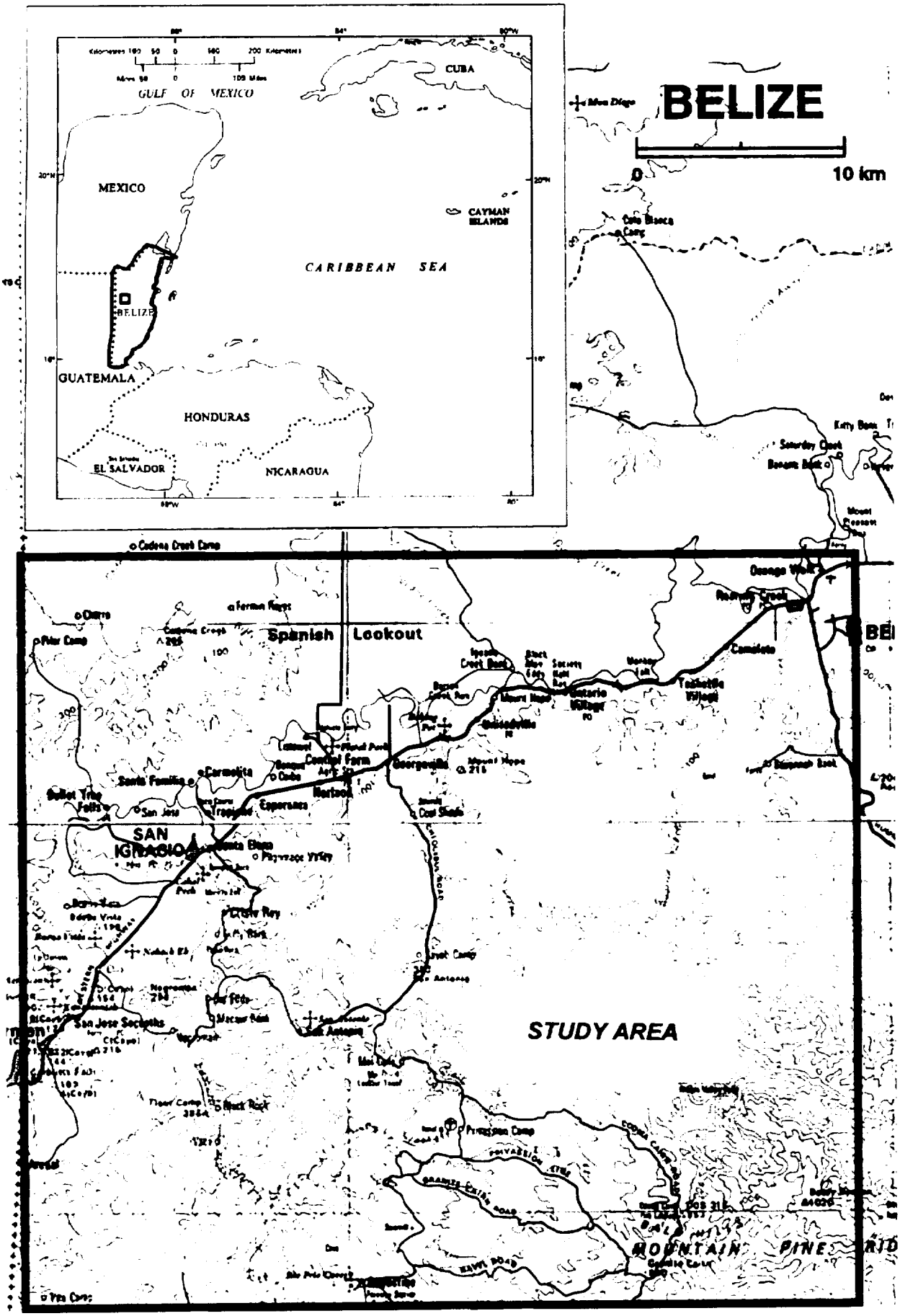

Figure 11. Map of the Cayo Distric study area in central Belize (outlined in black).

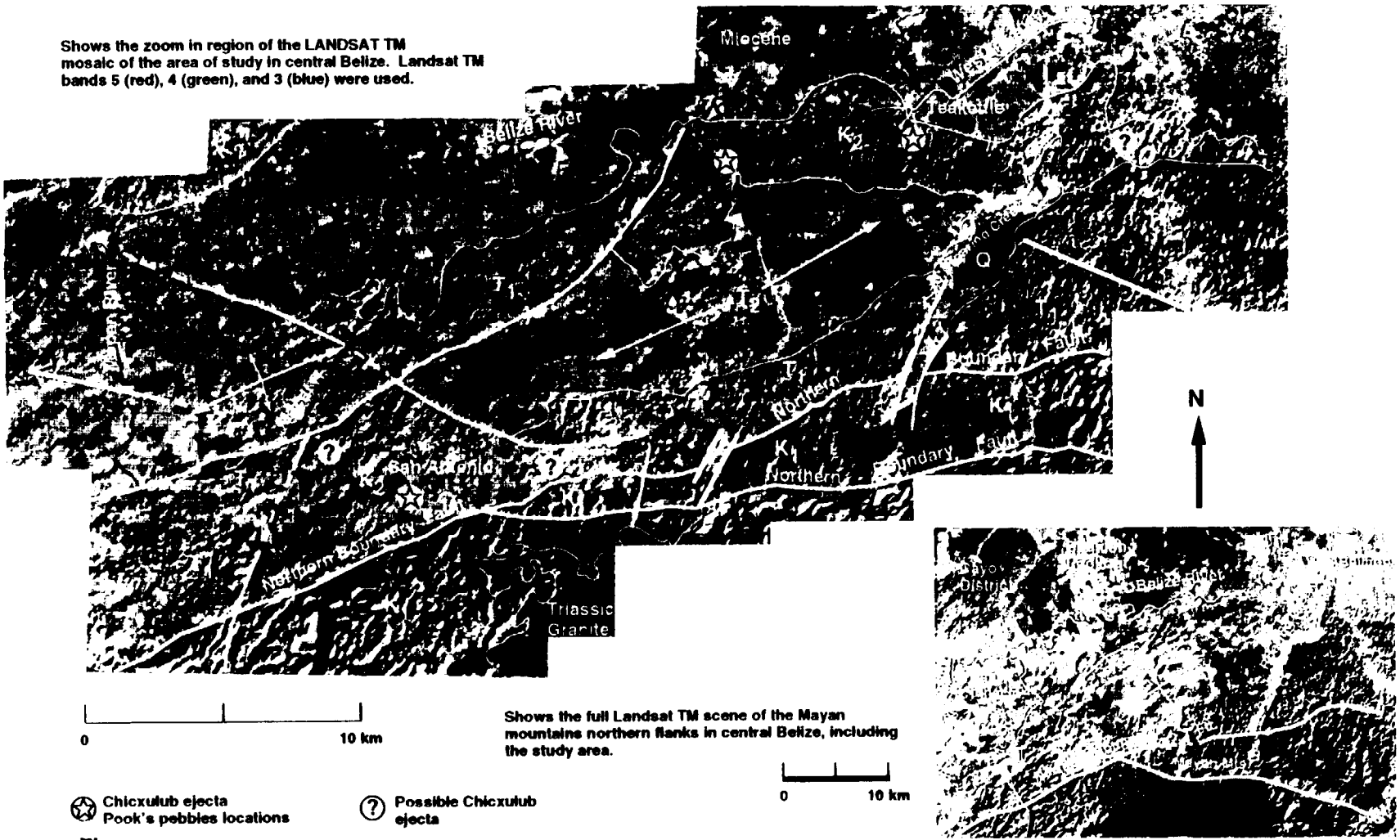

Figure 12. Landsat TM satellite image of Cayo study area. False color with band 5 in red, band 4 in green, and band 3 in blue. Shown in yellow are photointerpretations of faults (bold lines) and geological boundaries (fine lines) delineating two Cretaceous (K1, K2) and two Tertiary (T1, T2) units not identified in the provisional geological map (Fig. 2).

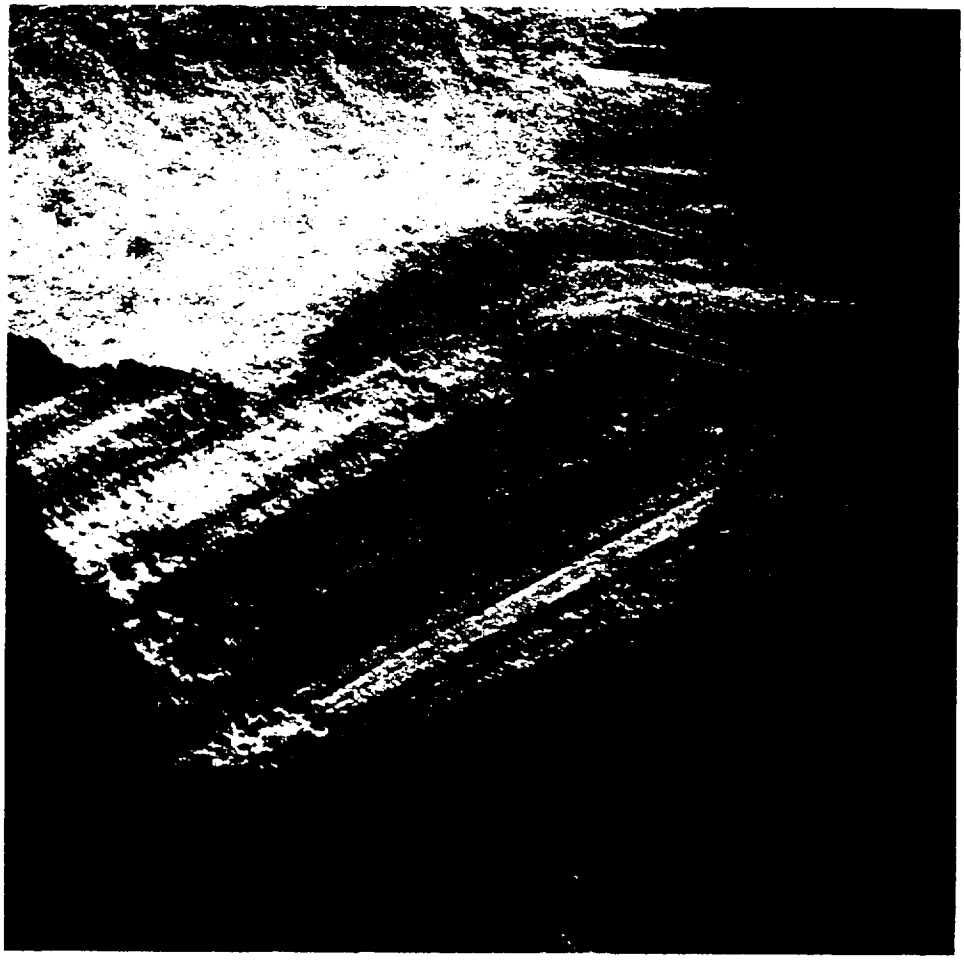

Figure 13. SEM image of multiple striations on Pook's Pebble. Cayo Diamictite.

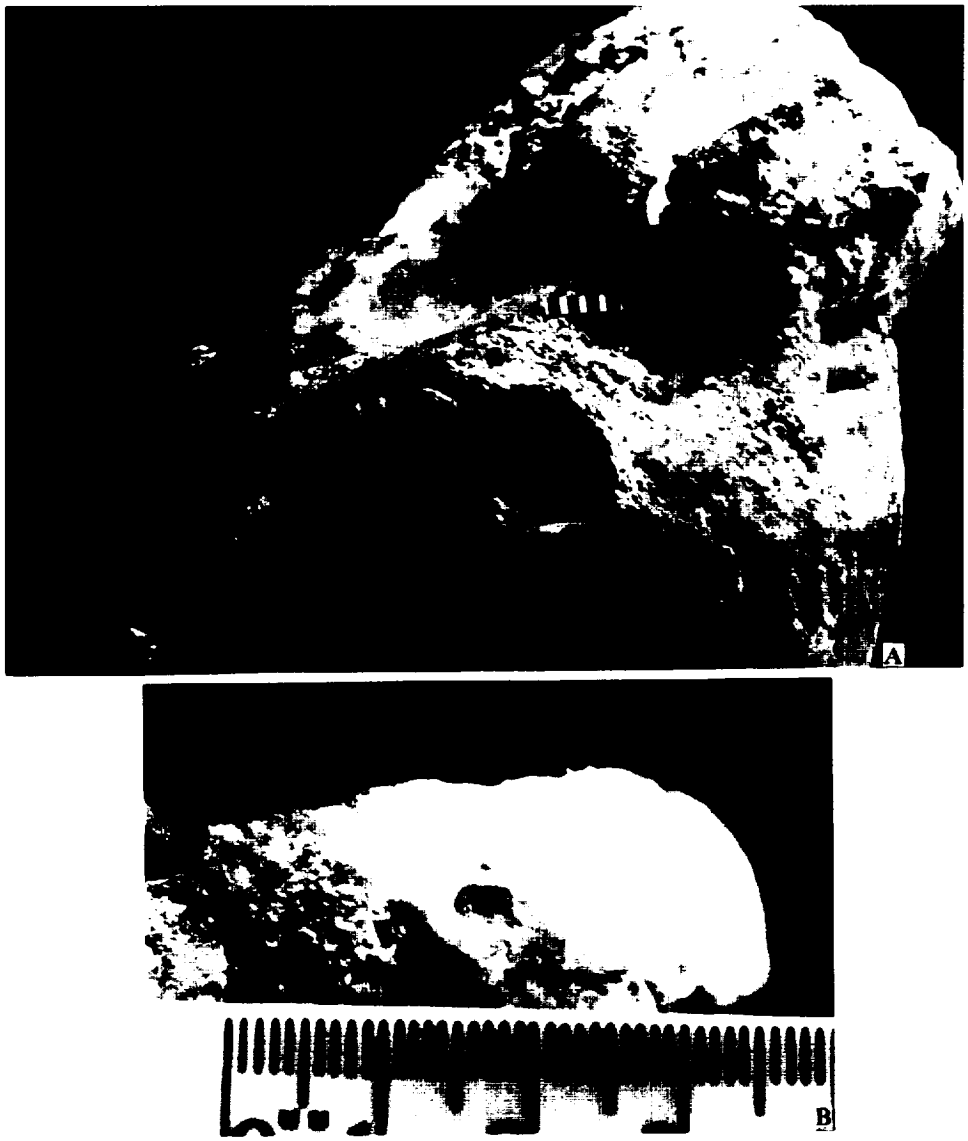

Figure 14. Pook's Pebbles. (A) Hand sample with crater, striations, and bleached chalcedony in relief and (B) highly polished surface with penetration pit. Cayo Diamictite.

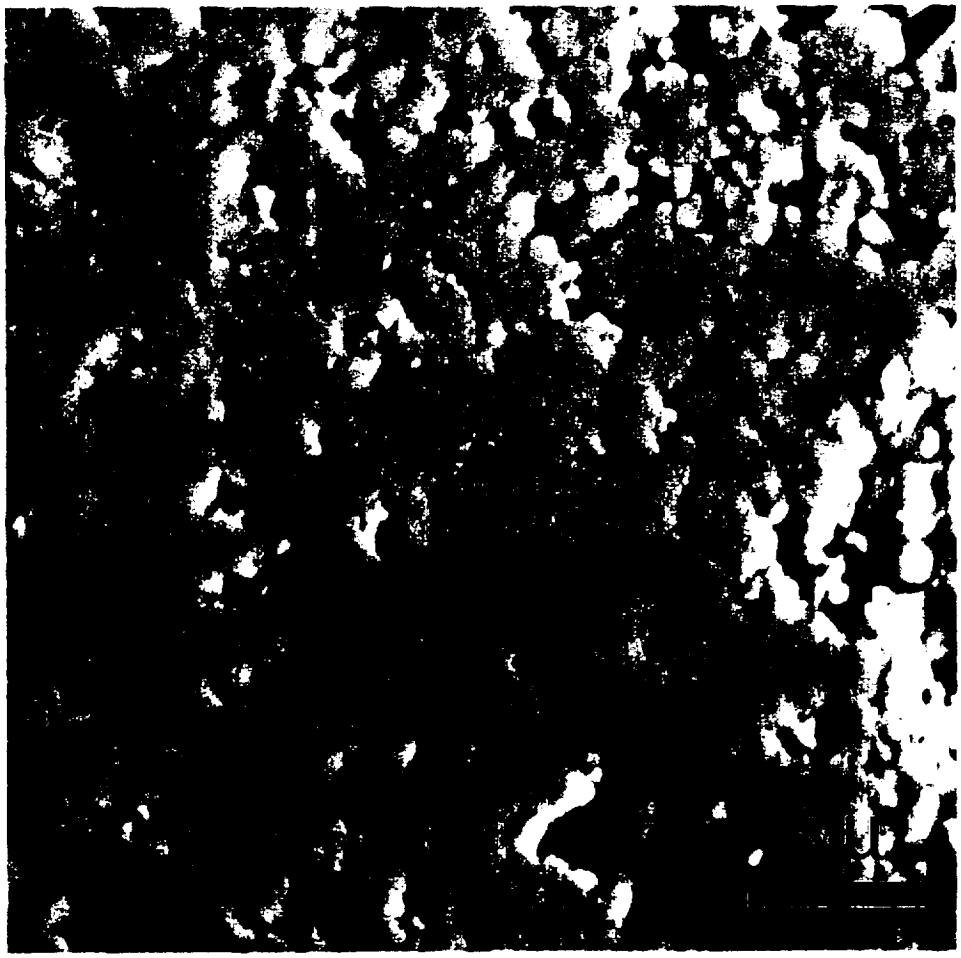

Figure 15. SEM of Pook's Pebble polished surface showing annealed crystal boundaries. Cayo Diamictite.

Lithology

Ejecta clasts exhibiting these unusual surface features are common in three Cayo K/T boundary sites and are composed of limestone (Pook's Pebbles). They are rare at the Albion Island site and are composed entirely of dolomite. The Pook's Pebbles are typically a microcrystalline pink limestone commonly containing veins and nodules of microspherulitic chalcedony and degraded microfossils (Figure 16). Microspherulitic chalcedony is also present at Albion Island, but is more rare. A few Pook's Pebbles with microspherulitic chalcedony were found where the chalcedony stands in high relief with a rough bleached surface surrounded by polished and striated limestone (Figure 14).

Interpretations

Ballistic calculations (ignoring atmosphere) require ejection velocities of 1-2 km/s to reach Belize, which produce trajectories that reach altitudes of 100 km (Figure 17). Atmospheric drag would reduce the range and thus require slightly higher ejection velocities. Impact models (Melosh, 1989) scaled to a 110 km diameter transient crater (the minimum appropriate for Chicxulub, see above) indicate that most (90%) of the ejecta with sufficient velocity to reach Belize would come from the 3 km thick sedimentary layer (Figure 18), which is composed of 70% carbonate and 30% sulfate (Ward et al., 1995). With the exception of spallation blocks, most of this ejecta would be shocked >10 GPa. Thus, theory alone predicts that the Belize ejecta should be dominated by moderately shocked carbonates. The lithological differences between Albion Island and Cayo may reflect ejection from different depths in the stratified carbonate platform at Chicxulub.

The curving striations and penetration features indicate that the carbonates deformed plastically. Plastic deformation of limestones may be possible under partial melting conditions of >100 bars and >1500°K (Tyburczy and Ahrens, 1986). These temperatures and pressures can be produced during the impact ejection phase, especially when the expanding vapor plume passes through the ejecta curtain (Vickery, 1986). It is also possible to reach partial melting conditions for limestones by ablation during atmospheric reentry (Schultz and Gault, 1982). Higher temperatures and pressures are required to melt dolomite (Wyllie and Huang, 1976), which might explain why these surface phenomena are rare at Albion Island where dolomites predominate.

We propose that the penetration features and many of the striations found on the Chicxulub carbonate ejecta clasts from Belize result from high velocity particle interactions under sufficient temperatures and pressures to partially melt the clast surfaces. The microspherulitic texture of the chalcedony may be a product of shock, as such textures are common in devitrified volcanic glass. We also propose that the calcite crusts and the fine polish are products of ablation that partially melted the surfaces and annealed crystal boundaries. Ablation of the limestones preferentially over the chalcedony may also explain the clasts where the encrusted chalcedony stands out in relief. Such ablation could occur either as the super heated vapor plume passes through the ejecta curtain, or when the high altitude ejecta re-enter the Earth's atmosphere. These results may prove important for understanding the effects of impact and high velocity ejection on carbonates in general. This is a critical issue in the study of possible fossil life in Martian meteorites that may have undergone a similar impact/ejection and Earth atmospheric reentry history.

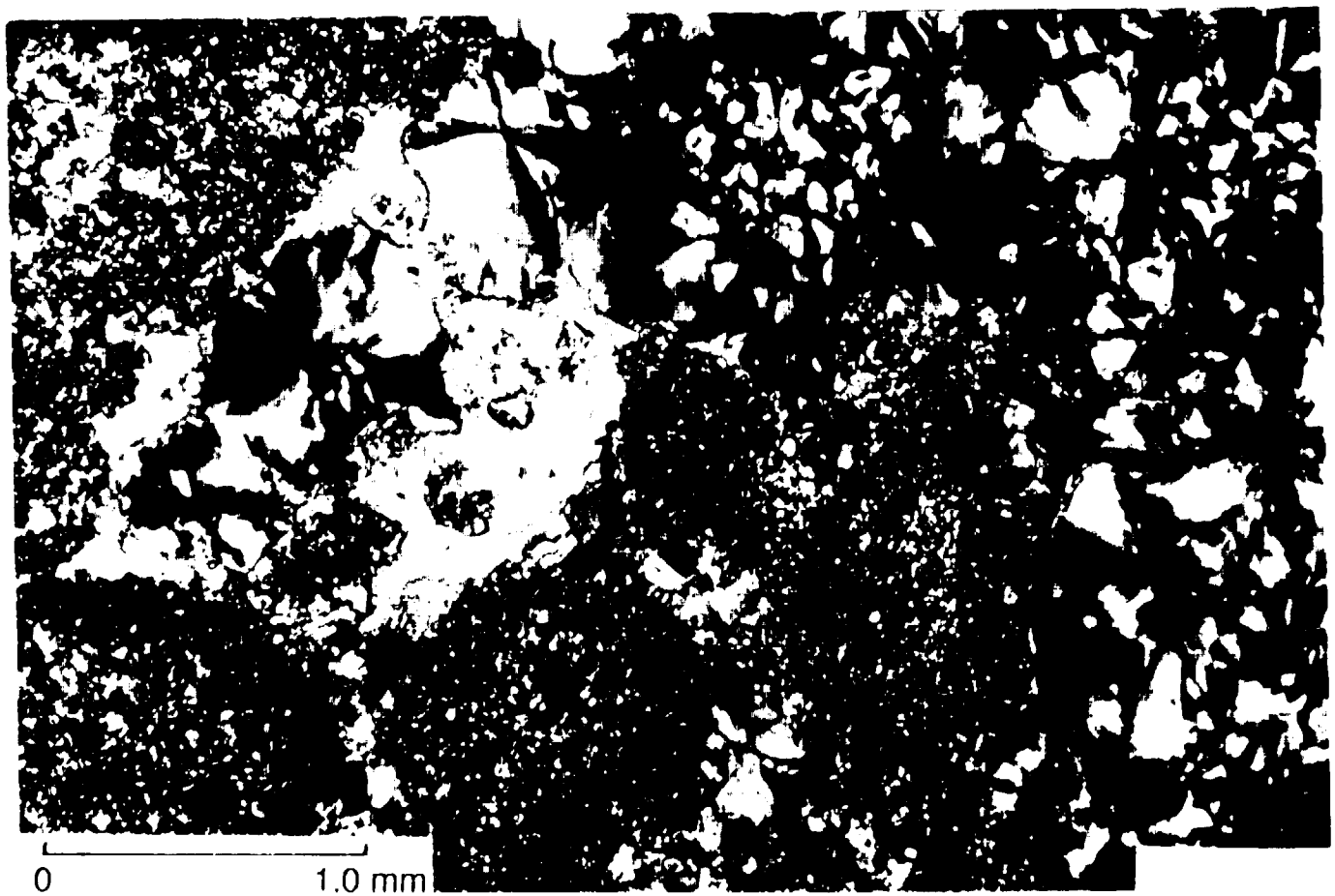

Figure 16. Thin section of Pook's Pebble showing microspherulitic chalcedony.

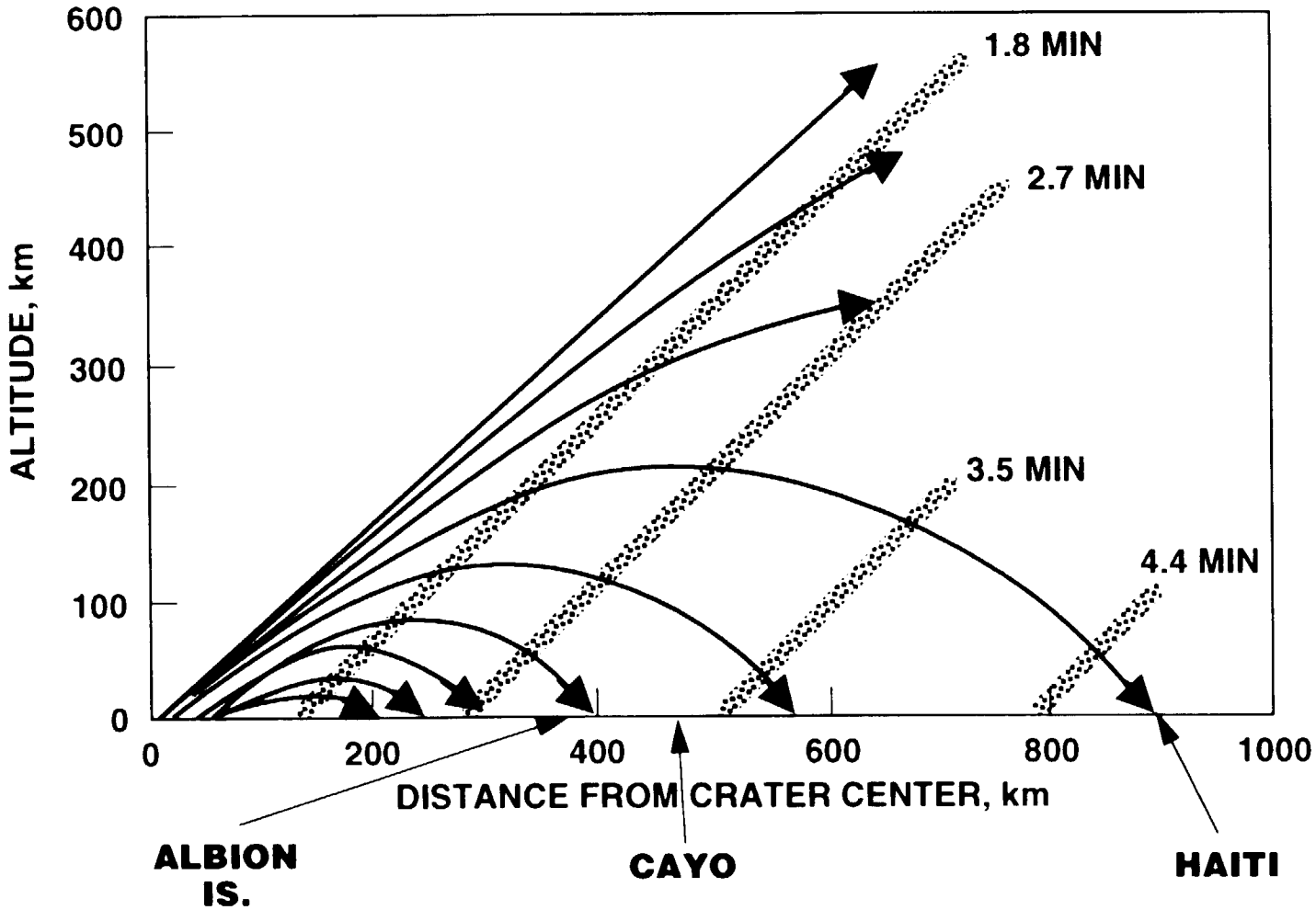

Figure 17. Ballistic trajectories for Chicxulub impact ejecta that reach Belize. Arrows show ballistic flight and purple dotted lines show distance traveled by ejecta curtain for various times after impact.

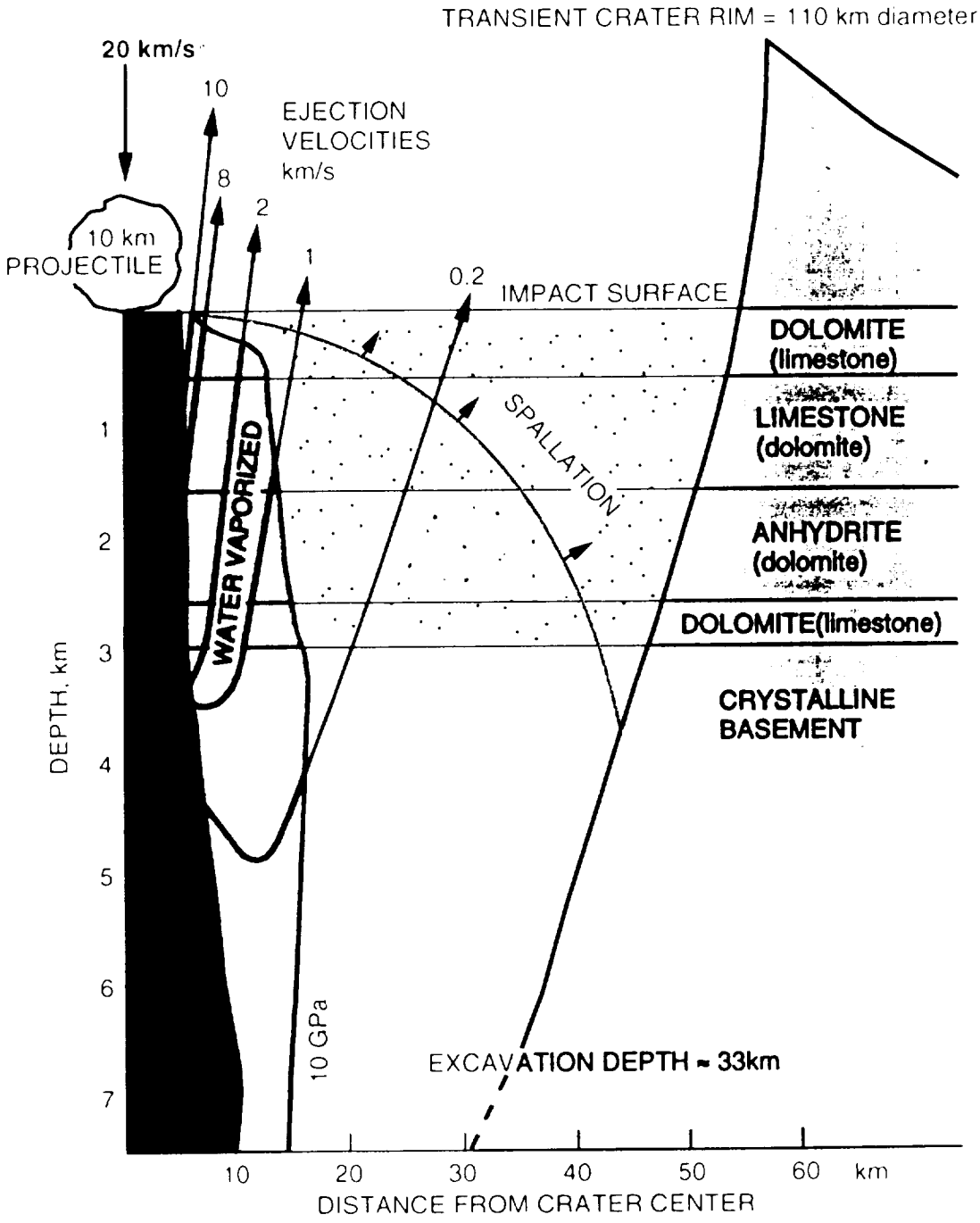

Figure 18. 2-D model (right half only) of the Chicxulub impact. Model is for a 10 km projectile impacting vertically at 20 km/s forming a transient crater 110 km in diameter. All rock within the red zone is vaporized or melted; all pore water within blue zone is vaporized. Stippled area represents sedimentary layers, labled at right. Curved green line demarcates spalation zone where rocks are ejected at high velocities with little shock. Black arrows show paths of high-speed ejecta: numbers at arrow tips give ejection velocites. Adapted from Melosh (1989).

REFERENCES

Alvarez, W., P. Claeys, and S. Kieffer, Emplacement of Cretaceous-Tertiary boundary shocked quartz from Chicxulub crater, Science, 269, 930-935, 1995.

Badjukov, D.D., Yu.P. Dikov, T.L. Petrova, and S.V. Pershin, Shock behavior of calcite, anhydrite, and gypsum (abstract), Lunar Planet. Sci., XXVI, 63-64, 1995.

Baines, K.H., and H.B. Hammel, Clouds, haze, and the stratospheric methane abundance in Neptune, Icarus, 109, 20-39, 1994.

Baines, K.H., and W.H. Smith, The atmospheric structure and dynamical properties of Neptune derived from ground-based and IUE spectrophotometry, Icarus, 85, 65-108, 1990.

Bard, J.P., Microtextures of igneous and metamorphic rocks: Boston, D. Reidel Pub. Co., 264 p., 1986.

Barnouin-Jha, O.S., and Schultz, P.H., Ejecta entrainment by impact-generated ring vortices: Theory and experiments, Journal of Geophysical Research, 101, 21,099-21,115, 1996.

Bohor, B.F., and B.P. Glass, Origin and diagenesis of K/T impact spherules: From Haiti to Wyoming and beyond, Meteoritics, 30, 182-198, 1995.

Chao, E.C.T., Huttner, R., and Schmidt-Kaler, H., Principal Exposures of the Ries Meteorite Crater in Southern Germany: Munchen, Bayerisches Geologisches Landesamt, 84 p., 1978.

Charlson, R.J., S.E. Schwartz, J.M. Hales, R.D. Cess, J.A. Coakley Jr., J.E. Hansen, and D.J. Hofmann, Climate forcing by anthropogenic Aerosols, Science, 255, 423-430, 1992.

Chaussidon, M., H. Sigurdsson, and N. Metrich, Sulfur and boron isotope study of high-Ca impact glasses from the K/T boundary: Constraints on source rocks, in The Cretaceous-Tertiary Event and Other Catastrophes in Earth History, edited by G. Ryder, D. Fastovsky, and S. Gartner, Spec. Pap. Geol. Soc. Am., 307, 253-262, 1996.

Claeys, P., Asaro, F., Rocchia, R., Robin, E., Hildebrand, A.R., Grajales, J.M., and Cedillo, E., Ir abundances in the Chicxulub melt-rock, in Montanari, A., and Coccioni, R., eds., The effects of impacts on the atmosphere and biosphere with regard to short- and long-term changes: Abstracts and Field Trips of the European Science Foundation 4th International Workshop of the Science Network on Impact Cratering and Evolution of Planet Earth, Ancona, p. 55-57, 1995.

Cornfield, R.M., Paleocene oceans and climate: An isotopic perspective, Earth Sci. Rev., 37, 225-252, 1994.

Croft, S.K., The scaling of complex craters, Proc. Lunar Planet. Sci. Conf. 15th, Part 2, J. Geophys.

Res., 90, suppl., C828-C842, 1985.

Fisher, R.V., and Schmincke, H., Pyroclastic Rocks: Berlin, Springer Verlag, 472 p., 1984.

Flores, G., Geology of northern British Honduras: American Association of Petroleum Geologists Bulletin, v. 36, p. 404-409, 1952.

Fouke, B.W., Alvarez, W., Claeys, Ph., Ocampo, A., Pope, K.O., Smit, J., and Vega, F.J., Cathodoluminesence study of carbonate growth phases in bedrock and KT ejecta from the Chicxulub Impact, at the Albion Island quarry, Belize: Geological Society of America Abstracts with Programs, v. 28, p. A-183, 1996a.

Fouke, B.W., Everts, A.-J.W., Zwart, E.W., Schlager, W., Smalley, P.C., and Weissert, H., Subaerial exposure unconformaties on the Verrcors carbonate plarform (SE France) and their sequence stratigraphic significance, in Howell, J.A., and Aitken, J.F., eds., High Resolution Sequence Stratigraphy: Innovations and Applications: Geological Society Publication, no. 104, p. 295-320, 1996b.

Gerasimov, M.V., Y.P. Dikov, O.I. Yakovlev, and F. Wlotzka, High-temperature vaporization of gypsum and anhydrite: Experimental results (abstract), Lunar Planet. Sci., XXV, 413-414, 1994.

Gerasimov, M.V., Y.P. Dikov, O.I. Yakovlev, and F. Wlotzka, High-temperature vaporization of quartz-calcite-anhydrite/gypsum targets in relation to Chicxulub impact (abstract), Lunar Planet. Sci., XXVI, 451-452, 1995.

Grajales N., J.M., Moran, D.J., Padilla, P., Sanchez, M.A., Cedillo, E., and Alvarez, W., The Loma Tristes Breccia: A K/T impact-related breccia from southern Mexico: Geological Society of America Abstracts with Programs, v. 28, p. A-183, 1996.

Graup, G., Terrestrial chondrules, glass spherules and accretionary lapilli from the suevite, Ries crater, Germany: Earth and Planetary Science Letters 45, 407-418, 1981.

Horz, F., Gall, H., Huttner, R., and Oberbeck, V.R., Shallow drilling in the "Bunte Breccia" impact deposits of the Ries Crater, Germany, in Roddy, D.J., Pepin, R.O., and Merril, R.B., eds., Impact and Explosion Cratering: New York, Pergamon Press, p. 425-448, 1977.

Horz, F., Ostertag, R., and Rainey, D.A., Bunte Breccia of the Ries: Continuous deposits of large impact craters: Reviews of Geophysics and Space Physics, 21, 1667-1725, 1983.

Hoff, R., Differential SO_2 column measurements of the Mt. Pinatubo volcanic plume, Geophys. Res. Lett., 19, 175-178, 1992.

Hollis, C.J., K.A. Rodgers, and R.J. Parker, Siliceous plankton bloom in the earliest Tertiary of Marlborough, New Zealand, Geology, 23, 835-838, 1995.

Hsu, K.J., and J.A. McKenzie, A "strangelove" ocean in the earliest Tertiary, in The Carbon Cycle and Atmospheric CO_2: Natural Variations, Archean to Present, Geophys. Monogr. Ser., vol. 32, edited by E.T. Sundquist and W.S. Broecker, pp. 487-492, AGU, Washington. D.C., 1985.

Hsu, K.J., and J.A. McKenzie, Carbon isotope anomalies at era boundaries; Global catastrophes and their ultimate cause, in Global Catastrophes in Earth History, edited by V.L. Sharpton and P.D. Ward, Spec. Pap. Geol. Soc. Am., 247, 61-70, 1990.

Ivanov, B.A., D.D. Badjukov, O.I. Yakovlev, M.V. Gerasimov, Yu.P. Dikov, K.O. Pope, and A.C. Ocampo, Degassing of sedimentary rocks due to Chicxulub impact: Hydrocode and physical simulations, in The Cretaceous-Tertiary Event and Other Catastrophes in Earth History, edited by G. Ryder, D. Fastovsky, and S. Gartner, Spec. Pap. Geol. Soc. Am., 307, 125-139, 1996.

Izett, G.A., Tektites in Cretaceous-Tertiary boundary rocks on Haiti and their bearing on the Alvarez impact extinction hypothesis, J. Geophys. Res. 96, 20,879-20,905, 1991.

Johnson, K., and P. Wilf, Paleobotanical temperature curve for the Cretaceous-Tertiary boundary interval and a scenario for the revegetation of North America after the terminal Cretaceous event, Geol. Soc. Amer. Abstr. Programs., 28, A225, 1996.

Kieffer, S.W., and C.H. Simonds, The role of volatiles and lithology in the impact cratering process, Rev. Geophys., 18, 143-181, 1980.

Koeberl, C., and Sigurdsson, H., Geochemistry of impact glasses from the K/T boundary in Haiti: Relation to smectites and a new type of glass: Geochimica et Cosmochemica Acta, 56, 2113-2129, 1992.

Kring, D.A., and Boynton, W.V., Altered spherules of impact melt and associated relic glass from the K/T boundary sediments in Haiti: Geochimica et Cosmochemica Acta, 55, 1737-1742, 1991.

Kyte, F.T., J. Smit, and J.T. Wasson, Siderophile interelement variations in the Cretaceous-Tertiary boundary sediments from Caravaca, Spain, Earth Planet. Sci. Lett., 73, 183-195, 1985.

Lyons, J.R., and T.J. Ahrens, Chicxulub impact-induced vaporization: S and C species and their affect on global climate (abstract), Lunar Planet. Sci., XXVII, 787-788, 1996.

Macdougall, J.D., Seawater strontium isotopes, acid rain, and the Cretaceous-Tertiary boundary, Science, 239, 485-487, 1988.

Marin, L.E., and V.L. Sharpton, Results of shallow drilling on the southern inner flank of the Chicxulub impact basin: Implications for basin size, Meteorit. Planet. Sci., 31, suppl., A82, 1996.

Martin, E.E., and J.D. Macdougall, Seawater SR isotopes at the Cretaceous/Tertiary boundary, Earth Planet. Sci. Lett., 104, 166-180, 1991.

Melosh, H.J., Impact Cratering: A Geologic Process, 245 pp., Oxford Univ. Press, New York, 1989.

Mroz, E.J., A.S. Mason, and W.A. Sedlacek, Stratospheric sulfate from El Chichon and the mystery volcano, Geophys. Res. Lett., 10, 873-876, 1983.

Ocampo, A.C., K.O. Pope, and A.G. Fischer, Ejecta blanket deposits of the Chicxulub crater from Albion Island, Belize, in The Cretaceous-Tertiary Event and Other Catastrophes in Earth History, edited by G. Ryder, D. Fastovsky, and S. Gartner, Spec. Pap. Geol. Soc. Am., 307, 75-88, 1996a.

Ocampo, A.C., and 8 others, Belize K/T boundary deposits: Relation to Chicxulub impact, Ejecta blanket deposits: Geological Society of America Abstracts with Programs, 28, A-182, 1996b.

Ocampo, A.C., Pope, K.O., and Fischer, A.G., Carbonate ejecta from the Chicxulub crater: Evidence for ablation and particle interaction under high temperatures and pressures: Lunar and Planetary Science, 28 CD, abstract 1861, 1997.

Pierazzo, E., H.J. Melosh, and D.A. Kring, Numerical simulation of the Chicxulub impact event (abstract), Lunar Planet. Sci., XXVII, 1029-1030, 1996.

Pinto, J.P, R.P. Turco, and O.B. Toon, Self-limiting physical and chemical effects in volcanic eruption clouds, J. Geophys. Res., 94, 11,165-11,174, 1989.

Pollack, J.B., D. Rind, A. Lacis, J.E. Hansen, M. Sato, and R. Ruedy, GCM simulations of volcanic aerosol forcing, I, Climate changes induced by steady-state perturbations, J. Clim., 6, 1719-1742, 1993.

Pollastro, R.M., and B.F. Bohor, Origin and clay-mineral genesis of the Cretaceous/Tertiary boundary unit, western interior of North America, Clays Clay Miner., 41, 7-25, 1993.

Pope, K.O., A.C. Ocampo, and C.E. Duller, Surficial geology of the Chicxulub impact crater, Yucatan, Mexico, Earth Moon Planets, 63, 93-104, 1993.

Pope, K.O., K.H. Baines, A.C. Ocampo, and B.A. Ivanov, Impact winter and the Cretaceous/Tertiary extinctions: Results of a Chicxulub asteroid impact model, Earth Planet. Sci. Lett., 128, 719-725, 1994.

Pope, K.O., A.C. Ocampo, G.L. Kinsland, and R. Smith, Surface expression of the Chicxulub crater, Geology, 24, 527-530, 1996.

Prasad, M.S., and Sudhakar, M., Collisions in the ejecta plume of the Australasian impact event: Lunar and Planetary Science, 27, 1053-1054, 1996.

Prinn, R.G., and B. Fegley, Bolide impacts, acid rain and biospheric traumas at the Cretaceous-

Tertiary boundary, Earth Planet. Sci Lett., 83, 1-15, 1987.

Rampino, M.R., and S. Self, Volcanic winter and accelerated glaciation following the Toba super-eruption, Nature, 359, 50-52, 1992.

Retallack, G.J., Acid trauma at the Cretaceous-Tertiary boundary in eastern Montana, GSA Today, 6, 1-7, 1996.

Rocchia, R., Claeys, P., and Robin, E., Lack of IR enrichment in the Chicxulub crater impact melt sheet: Eos Transactions, American Geophysical Union Fall Meeting Supplement, 75, 416, 1994.

Rose, W.I., and C.A. Chesner, Worldwide dispersal of ash and gases from earth's largest known eruption: Toba, Sumatra, 75 ka, Palaeogeogr. Palaeoclim. Palaeoecol. 89, 269-275, 1990.

Schultz, P., Effect of impact angle on vaporization, J. Geophys. Res., 101, 21,117-21,136, 1996.

Schultz, P.H., and D.E. Gault, Atmospheric effects on Martian ejecta emplacement: Journal of Geophysical Research, 84, 7669-7687, 1979.

Schultz, P.H., and D.E. Gault, Impact dynamics in an atmosphere: Experimental results and extrapolations, in Geological Implications of Impacts of Large Asteroids and Comets on the Earth, edited by L.T. Silver and P.H. Schultz, Geological Society of America Special Paper, 190, 153-174, 1982.

Schultz, P.H., and S. D'Hondt, Cretaceous-Tertiary (Chicxulub) impact angle and its consequences, Geology, 24, 963-976, 1996.

Schuraytz, B.C., Sharpton, V.L., and Marin, L.E., Petrology of impact-melt rocks at the Chicxulub multiring basin, Yucatan, Mexico: Geology, 22, 868-872, 1994.

Sharpton, V.L., K. Burke, A. Camargo-Zanoguera, S.A. Hall, D.S. Lee, L.E. Marin, G. Suarez-Reynoso, J.M. Quezada-Muneton, P.D. Spudis, and J. Urrutia-Fucugauchi, Chicxulub multiring impact basin: Size and other characteristics derived from gravity analysis, Science, 261, 1564-1567, 1993.

Sharpton, V.L., L.E. Marin, J.L. Carney, S. Lee, G. Ryder, B.C. Schuraytz, P. Sikora, and P.D. Spudis, A model of the Chicxulub impact basin based on evaluation of geophysical data, well logs and drill core samples, in The Cretaceous-Tertiary Event and Other Catastrophes in Earth History, edited by G. Ryder, D. Fastovsky, and S. Gartner, Spec. Pap. Geol. Soc. Am., 307, 55-74, 1996.

Sigurdsson, H., P. Bonte, L. Turpin, M. Chaussidon, N. Metrich, M. Steinberg, P. Pradel, and S. D'Hondt, Geochemical constraints on source region of Cretaceous/Tertiary impact glasses, Nature, 353, 839-842, 1991a.

Sigurdsson, H., S. D'Hondt, M.A. Arthur, T.J. Bralower, J.C. Zachos, M. van Fossen, and J.E.T. Channell, Glass from the Cretaceous/Tertiary boundary in Haiti, Nature, 349, 482-487, 1991b.

Sigurdsson, H., S. D'Hondt, and S. Carey, The impact of the Cretaceous/Tertiary bolide on evaporite terrain and the generation of major sulfuric acid aerosol, Earth Planet. Sci. Lett., 109, 543-559, 1992.

Smit, J., T.B. Roep, W. Alvarez, A. Montanari, P. Claeys, J.M. Grajales-Nashiimura, and J. Bermudez, Coarse-grained clastic sandstone complex at the K/T boundary around the Gulf of Mexico: Deposition by tsunami waves induced by the Chicxulub impact?, in The Cretaceous-Tertiary Event and Other Catastrophes in Earth History, edited by G. Ryder, D. Fastovsky, and S. Gartner, Spec. Pap. Geol. Soc. Am., 307, 151-182, 1996.

Takata, T., J.D. O'Keefe, T.J. Ahrens, and G.S. Orton, Comet Shoemaker-Levy 9: Impact on Jupiter and plume evolution, Icarus, 109, 3-19, 1994.

Toon, O.B., J.B. Pollack, T.P. Ackerman, R.P. Turco, C.P. McKay, and M.S. Liu, Evolution of an impact-generated dust cloud and its effects on the atmosphere, in Geological Implications of Impacts of Large Asteroids and Comets on Earth, edited by L.T. Silver and P.H. Schultz, Spec. Pap. Geol. Soc. Am., 190, 187-200, 1982.

Tyburczy, J.A., and T.J. Ahrens, Dynamic compression and volatile release of carbonates, J. Geophys. Res., 91, 4730-4744, 1986

Vega, F.J., R.M. Feldman, A.C. Ocampo, K.O. Pope, A new species of Late Cretaceous carcineretid crab (Brachyura: Carcineretidae) from Albion Island, Belize: Journal of Paleontology, in press.

Vickery, A.M., Effect of an impact-generated gas cloud on the acceleration of solid ejecta: Journal of Geophysical Research, 91, 14,139-14,160, 1986.

Vickery, A.M., The theory of jetting: Application to the origin of tektites: Icarus, 105, 441-453, 1993.

Vickery, A.M., and H.J. Melosh, Atmospheric erosion and impactor retention in large impacts, with application to mass extinction, in Global Catastrophes in Earth History, edited by V.L. Sharpton and P.D. Ward, Spec. Pap. Geol. Soc. Am., 247, 289-300, 1990.

Ward, W.C., G. Keller, W. Stinnesbeck, and T. Adatte, Yucatan subsurface stratigraphy: Implications and constraints for the Chicxulub impact, Geology, 23, 873-876, 1995.

Wyllie, P.J., and W.L. Huang, Carbinaion and melting reactions in the system CaO-MgO-SiO_2-CO_2 at mantle pressures with geophysical and petrological applications, Contributions to Mineralogy and Petrology, 54, 79-107, 1976.

Yang, W., T.J. Ahrens, and G. Chen, Shock vaporization of anhydrite and calcite and the effects on

global climate from the K/T impact crater at Chicxulub (abstract), Lunar Planet. Sci., XXVII, 1473-1474, 1996.

Zachos, J.C., M.A. Arthur, and W.E. Dean, Geochemical evidence for suppression of pelagic marine productivity at the Cretaceous/Tertiary boundary, Nature, 337, 61-64, 1989.

Zahnle, K.J., Atmospheric chemistry by large impacts, in Global Catastrophes in Earth History, edited by V.L. Sharpton and P.D. Ward, Spec. Pap. Geol. Soc. Am., 247, 271-288, 1990.

Zahnle, K., and M.-M. MacLow, The collision of Jupiter and comet Shoemaker-Levy 9, Icarus, 108, 1-17, 1994.

Zahnle, K., M.-M. MacLow, K. Lodders, and B. Fegley Jr., Sulfur chemistry in the wake of comet Shoemaker-Levy 9, Geophys. Res. Lett., 22, 1593-1596, 1995.

Zielinski, G.A., P.A. Mayewski, L.D. Meeker, S. Whitlow, M.S., Twickler, and K. Taylor, Potential atmospheric impact of the Toba mega-eruption ~71,000 years ago, Geophys. Res. Lett., 23, 837-840, 1996.

REPORT DOCUMENTATION PAGE

Form Approved
OMB No. 0704-0188

1. AGENCY USE ONLY (Leave blank)	2. REPORT DATE	3. REPORT TYPE AND DATES COVERED
	8/14/97	10/1/96 — 8/1/97

4. TITLE AND SUBTITLE
Annual Report Contract NASW 96030

5. FUNDING NUMBERS

6. AUTHOR(S)
Kevin O. Pope

7. PERFORMING ORGANIZATION NAME(S) AND ADDRESS(ES)
Geo Eco Arc Research
2222 Foothill Blvd. Suite E-272
La Cañada, CA 91011 USA

8. PERFORMING ORGANIZATION REPORT NUMBER

9. SPONSORING/MONITORING AGENCY NAME(S) AND ADDRESS(ES)
National Aeronautics and Space Administration
Code SR
Washington, DC 20546-0001

10. SPONSORING/MONITORING AGENCY REPORT NUMBER
NASW 96030

11. SUPPLEMENTARY NOTES

12a. DISTRIBUTION/AVAILABILITY STATEMENT

12b. DISTRIBUTION CODE

13. ABSTRACT *(Maximum 200 words)*

A comprehensive analysis of volatiles in the Chicxulub impact strongly supports the hypothesis that impact-generated sulfate aerosols caused over a decade of global cooling, acid rain, and disruption of ocean circulation, which contributed to the mass extinction at the Cretaceous/Tertiary (K/T) boundary. The crater size, meteoritic content of the K/T boundary clay, and impact models indicate that the Chicxulub crater was formed by a short period comet or an asteroid impact that released 0.7-3.4 x 10^{31} ergs of energy. Impact models and experiments combined with estimates of volatiles in the projectile and target rocks predict that over 200 gigatons (Gt) each of SO_2 and water vapor, and over 500 Gt of CO_2, were globally distributed in the stratosphere by the impact.

14. SUBJECT TERMS	15. NUMBER OF PAGES
Impact crater, Climate Change	25
	16. PRICE CODE

17. SECURITY CLASSIFICATION OF REPORT	18. SECURITY CLASSIFICATION OF THIS PAGE	19. SECURITY CLASSIFICATION OF ABSTRACT	20. LIMITATION OF ABSTRACT
None	None	None	None